False Arrhythmia Alarm Suppression Using ECG, ABP, and Photoplethysmogram

by

Anagha Vishwas Deshmane

S.B., Massacusetts Institute of Technology (2008)

Submitted to the Department of Electrical Engineering and Computer Science
in partial fulfillment of the requirements for the degree of

Master of Engineering in Electrical Engineering and Computer Science

at the

MASSACHUSETTS INSTITUTE OF TECHNOLOGY

September 2009

Author .....
Department of Electrical Engineering and Computer Science
August 21, 2009

Certified by .....
Dr. Roger G. Mark
Distinguished Professor in Health Science & Technology
M.I.T. Thesis Supervisor

Certified by .....
Lauren J. Kessler
Charles Stark Draper Laboratory
VI-A Company Thesis Supervisor

Accepted by .....
Dr. Christopher J. Terman
Chairman, Department Committee on Graduate Theses

False Arrhythmia Alarm Suppression Using ECG, ABP, and Photoplethysmogram

by

Anagha Vishwas Deshmane

Submitted to the Department of Electrical Engineering and Computer Science
on August 21, 2009, in partial fulfillment of the
requirements for the degree of
Master of Engineering in Electrical Engineering and Computer Science

Abstract

A signal quality assessment scheme for the photoplethysmogram waveform recorded by a pulse oximeter has been created. The signal quality algorithm uses statistical methods on time-series and spectral analysis to locate high-frequency segments of the photoplethysmogram waveform. A photoplethysmogram pulse onset detector has been implemented for heart rate estimation. Application of the signal quality metric and photoplethysmogram pulse onset detector are demonstrated in an algorithm which suppresses false electrocardiogram critical arrhythmia alarms issued by bedside monitors in hospital intensive care units.

M.I.T. Thesis Supervisor: Dr. Roger G. Mark
Title: Distinguished Professor in Health Science & Technology

VI-A Company Thesis Supervisor: Lauren J. Kessler
Affiliation: Charles Stark Draper Laboratory

Acknowledgments

I would like to thank Dr. Roger Mark and Dr. Gari Clifford for sharing their medical insight, engineering expertice, and guidance on the general direction of this research. Thanks to Omar Abdala for his discussions on Hjorth parameters, and Daniel Scott and Mauricio Villarroel for their extensive computing knowledge and help with navigating the MIMIC II database and related tools. Thanks to the members of the Bioengineering Research Partnership for their feedback during group meetings. Last but not least, I would like to express my deepest gratitude to my VI-A advisor, Lauren Kessler, for several years of encouragement, excellent mentorship, and guidance during the thesis-writing process.

Thanks to the members of the Lab for Computational Physiology at M.I.T. for making my time in the lab enjoyable, and teaching me how to take a lunch break and get addicted to coffee. Special thanks to the resident students, Tiffany Chen and Shamim Nemati, and the visiting students, Violetta Monastario Bazin and Patti Ordonez Rozo, for keeping me company during nights and weekends in the lab, and providing endless hours of amusement.

Finally, I would like to thank my parents, Vishwas and Meera, and my sister, Anisha, for a lifetime of inspiration, encouragement, and continued support of all my endeavors.

This work was funded in part through the Draper Fellows program at the Charles Stark Draper Laboratory, under contract numbers 22951-0001 and 23985-001. Publication of this thesis does not constitute approval by the Charles Stark Draper Laboratory. It is published for the exchange and stimulation of ideas.

The work described here was also supported by Grant Number RO1-EB001659 from the National Institute of Biomedical Imaging and Bioengineering. The content is solely the responsibility of the author and does not necessarily represent the official views of the National Institute of Biomedical Imaging and Bioengineering or the National Institutes of Health.

THIS PAGE INTENTIONALLY LEFT BLANK

Contents

THIS PAGE INTENTIONALLY LEFT BLANK

List of Figures

List of Tables

Chapter 1

Introduction

1.1 Motivation and Background

Falsely issued alarms in intensive care units (ICUs) disrupt patients' rest, drain hospital resources, and desensitize the hospital staff to potential emergency situations [2]. It has been estimated that 43% of life-threatening electrocardiogram (ECG) alarms issued by bedside monitors are false, with some categories of alarm being as high as 90% [1]. These false arrhythmia alarms are often triggered by noise and other artifacts in the monitored ECG waveform, and can be suppressed in the presence of other data which indicate that there are no critical abnormalities in cardiac function. Such information can come from signals which are related to cardiac function but are measured in a location remote to the heart and are therefore unlikely to exhibit the same types of noise and artifacts as the ECG. Signals with pulsatile waveforms offer the additional benefit of having features indicative of the cardiac cycle, which can be later compared to timing and morphology of features in the ECG waveform.

Aboukhalil *et al.* have created an algorithmic framework which consults the arterial blood pressure (ABP) waveform to corroborate critical ECG arrhythmia alarms [1, 3]. If an ECG alarm is triggered, the algorithm checks the signal quality of the simultaneously recorded ABP waveform. If this waveform is of poor quality, the ECG alarm is accepted as true. If the ABP signal is of high quality, the algorithm checks that the features extracted from the blood pressure waveform corroborate the condi-

tion which triggered the ECG alarm. The alarm is suppressed if the blood pressure waveform does not exhibit features consistent with a cardiac arrhythmia.

The blood pressure signal quality assessment scheme in this framework, designed by Sun *et al.* [26], uses a binary signal abnormality index, $jSQI$, to indicate if each blood pressure beat is unsuitably noisy. The $jSQI$ algorithm detects the onset of each pulse in the blood pressure signal, and flags the beat as abnormal if its features, which include beat duration, systolic, diastolic, mean, and pulse pressures, do not fall within physiologically possible ranges. Zong *et al.* [33] had previously created a blood pressure signal quality metric, $wSQI$, which uses fuzzy logic to asses the extent to which the features of each ABP pulse fall within physiologically normal ranges, yielding a continuous signal quality index value between 0 (abnormal) and 1 (normal). Li *et al.* [15] used the two ABP signal quality measures for robust heart rate estimation from simultaneously recorded ECG and ABP waveforms by weighing each beat's $jSQI$ value by $wSQI$.

Zong *et al.* [33] note that while $jSQI$ and $wSQI$ are successful at assessing signal quality, they are limited by artifacts of the ABP measurement, such as those due to catheter flush. The availability of the arterial blood pressure waveform poses further limitations. We estimate that only 60% of adult ICU patients have ABP simultaneously recorded with ECG, due to the invasive nature of the measurement and simply because not all patients require arterial blood pressure monitoring. Zong *et al.* [33] suggest that the false critical ECG alarm suppression rate can be improved if the ECG is compared to multiple cardiac function indicators, so that if one signal is of poor quality, an alternate signal can be consulted. One source for such information is the photoplethysmogram (PPG) waveform, which is pulsatile and non-invasively obtained from a pulse oximeter affixed to the patient's finger (in the case of transmission pulse oximetry) or adhered to the skin (in reflective pulse oximetry). The PPG waveform has different noise characteristics from the arterial blood pressure waveform due to the difference in measurement technique and sensor location. For example, the PPG waveform measures blood flow further down the arterial tree from the site of the ABP measurement; as a result, the waveform resembles a delayed and

low-pass filtered version of the ABP waveform. A situation where the PPG waveform might provide more information than the ABP waveform to the alarm suppression framework is illustrated in Fig. 1-1. Here, the electrocardiogram waveform exhibits a premature ventricular beat pattern which triggered an alarm. The arterial blood pressure waveform is too noisy to consult for information to verify the ECG alarm. The photoplethysmogram waveform, however, shows low-amplitude beats in accordance with the premature beats which are inefficient at pumping blood.

Just as use of the information in the ABP waveform required blood pressure signal quality measures, incorporation of information extracted from the PPG waveform into the ECG false alarm suppression framework of Clifford *et al.* [3] requires assessment of PPG signal quality to avoid drawing misleading information from an artifactual waveform. The algorithms introduced in this thesis form a signal quality assessment scheme for the PPG waveform recorded by a pulse oximeter. These algorithms, which perform artifact detection, pulse onset identification, and pulse feature extraction, can be used to determine high-quality segments of the PPG waveform, which can be used to imporove false ECG alarm suppression and reduce true alarm suppression.

1.2 The Photoplethysmogram Waveform

1.2.1 Pulse Oximetry

Since its invention in the 1970s and commercial development in the 1980s, pulse oximetry has provided a non-invasive method of estimating functional oxygen saturation of the blood in clinical settings. Oximetry is based on the fact that hemoglobin absorbs light in limited frequency ranges.

Oxygen reversibly binds to hemoglobin in the blood in order to nourish tissues in the peripheral regions of the body. The oxygen is released from the blood and into the tissue at the capillary level of the cardiovascular system. When oxygen reversibly binds to hemoglobin, the resulting shift in the distribution of electrons in the hemoglobin molecule causes its optical properties to change [6]. In particu-

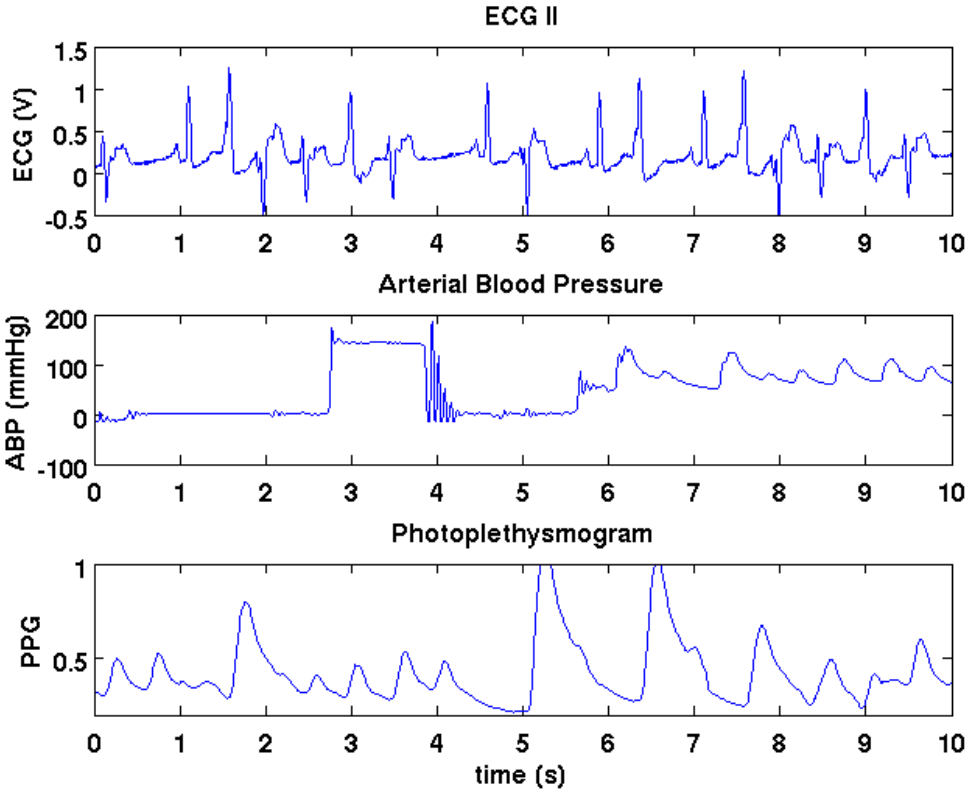

Figure 1-1: Using the photoplethysmogram to corroborate ECG alarms. In this segment of simultaneously recorded electrocardiogram, arterial blood pressure, and photoplethysmogram waveforms, an ECG monitor would issue an arrhythmia alarm due to premature ventricular beats. In this case, we would not be able to corroborate the alarm by consulting the arterial blood pressure waveform because of noise in the channel. However, the photoplethysmogram waveform does not exhibit noise and the morphology of its beats can be related to the shapes and timing of the electrocardiogram QRS complexes.

lar, oxygenated hemoglobin (O_2Hb) absorbs visible light in the blue region, making blood appear red. Reduced or deoxygenated hemoglobin (RHb) absorbs light at most frequencies in the visible spectrum, making blood appear dark (or blue when viewed through the layers of the skin). Permanent binding of carbon monoxide to hemoglobin, forming carboxyhemoglobin (COHb), and the binding of ferric ions to hemoglobin, forming methemoglobin (MetHb), also cause the hemoglobin absorption spectrum to shift for various frequencies of light. As illustrated in Fig. 1-2, the light absorption of O_2Hb and RHb differ most significantly in the red and near-infrared regions [27]. Pulse oximetry devices typically study the absorption of at least two

wavelengths of light, at approximately 660nm and 940nm, by measuring the amount of light transmitted through or reflected from perfused tissue such as that found in the finger, earlobe, or on the forehead.

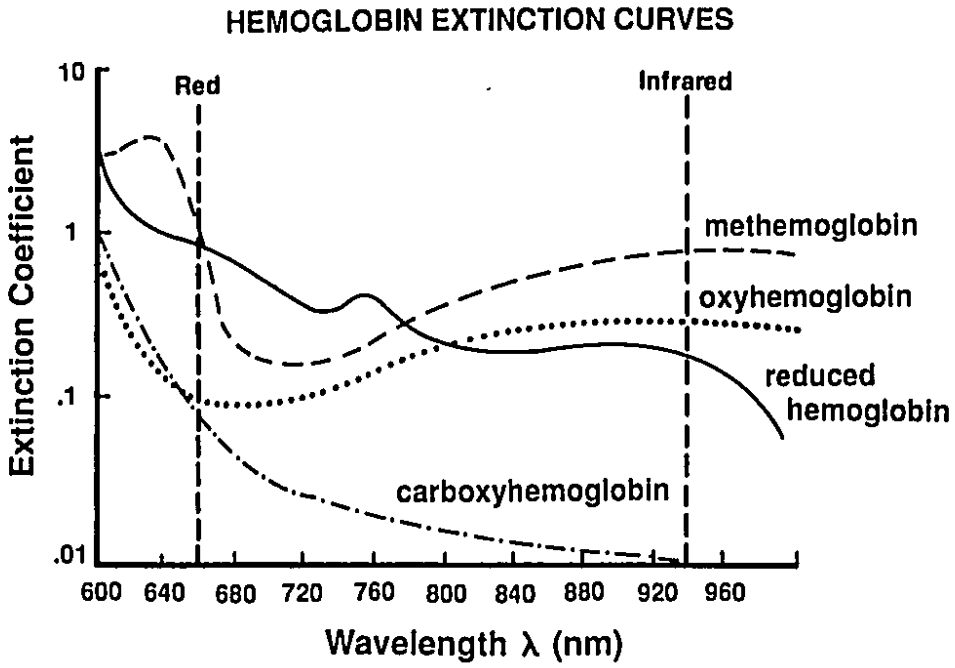

Figure 1-2: Absorption spectrum of hemoglobin species. Transmitted light absorption of oxyhemoglobin and deoxyhemoglobin (reduced hemoglobin) differs most significantly in the red and near-infrared frequencies. Note the extinction coefficients are plotted on a logarithmic scale. Adapted from Figure 2 in [27].

Transmission pulse oximetry is based on an estimation of the Beer-Lambert Law, which states that the intensity of light trasmitted through a material is proportional to the intensity of incident light and exponentially related to the amount of light absorbed. The amount of light absorbed by a sample, A, is a dimensionless quantity defined in terms of the light intensity in the presence of the sample, I (in W/m^2), and in the absence of the sample, I_0, as

$$A = -\log(\frac{I}{I_0}), \tag{1.1}$$

and is linearly proportional to the extinction coefficient and path length, expressed as

$$A = \epsilon c l, \tag{1.2}$$

where ϵ is the molar absorptivity (in m^2/mol) of the sample, c is the concentration (in mol/m^3) of the hemoglobin species, skin, muscle, and bone, and l is the path length in meters of the transmitted light [6].

In transmission pulse oximeters, one light-emmitting diode of each wavelength, 660 nm and 940 nm, shines incident at roughly 90° to the outer tissue (typically through the nail on the back of a finger tip for adults), and the intensity of the transmitted light is detected on the opposite side (typically the finger pad). For each frequency of incident light, the absorption can be expressed as a sum of absorption due to O_2Hb, RHb, COHb, and MetHb, as well as absorbtion by other non-blood sources, such as surrounding tissues. Finger probe pulse oximeters operate under the assumption that the path length l maintains a steady "direct current" (DC) value due to venous and arterial blood, as well as an alternating "current" (AC) component due to the expansion of the capillaries as each wave of blood is pumped from the heart and flows through the vasculature. The resulting absorption waveform is illustrated in Fig. 1-3. It has been noted that the AC component of these absorption waveforms account for less than 1% of the total light absorbed by the perfused tissue. Absorption measurements are highly susceptable to any change in the material surrounding the pulsating arterial vasculature, including the disturbance of muscle, skin, and venous blood in response to motion [22].

The pulsatile PPG waveform displayed on ICU monitors is a dimentionless quantity computed from a ratio comparing the AC amplitude to DC light absorption of the red and infrared wavelengths as follows [6, 27]:

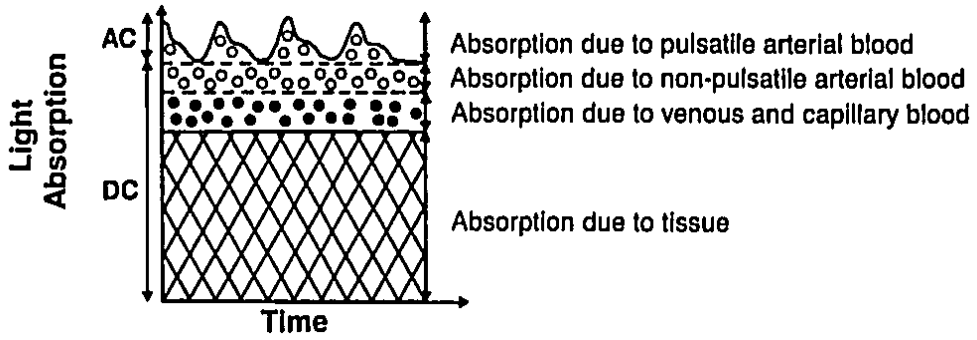

Figure 1-3: Light absorption waveform in inhomogenious tissue. In pulse oximetry, the AC component is due to the varying path length when the arterial vasculature expands during a pulse. Note this AC component only accounts for approximately 1% of the total absorption. Adapted from Figure 3 in [27].

$$R = \frac{dA_{660nm}/dt}{dA_{940nm}/dt} = \frac{AC_{660nm}/DC_{660nm}}{AC_{940nm}/DC_{940nm}}. \tag{1.3}$$

R is a pulsatile waveform taking values between 0 and 1, similar in appearance to the ABP.

From this ratio, an estimate of functional oxygen saturation in arterial blood can be made [6]. Substituting equations 1.1 and 1.2 into equation 1.3, and recalling that the pulsatile component of the signal is due to movement of oxyhemoglobin, R can also be expressed as follows:

$$R = \frac{\epsilon_{o,660nm}c_o + \epsilon_{r,660nm}c_r}{\epsilon_{o,940nm}c_o + \epsilon_{r,940nm}c_r} \tag{1.4}$$

where ϵ_o and c_o are the molar absorptivity and concentration of oxyhemoglobin, and ϵ_r and c_r are the molar absorptivity and concentration of reduced hemoglobin, respectively. Functional oxygen concentration is defined by $\%SaO_2 = c_o/(c_o + c_r)$. This allows us to express the theoretical relationship between $\%SaO_2$ as follows [6]:

$$\%SaO_2 = \frac{\epsilon_{r,660nm} - \epsilon_{r,940nm}R}{(\epsilon_{r,660nm} - \epsilon_{o,660nm}) - (\epsilon_{r,940nm} - \epsilon_{o,940nm})R} \tag{1.5}$$

Due to limitations to the Beer-Lambert law caused by light scattering in tissue and pulse oximeter device characteristics, the true relationship between pulsatile estimate of functional oxygen saturation, $\%SpO_2$ and R is empirically determined by fitting data from human volunteers to an equation of the form $S = (a - bR)/(c - dR)$ [6]. This relationship is illustrated in Figure 1-4. In addition to the waveform, R, the $\%SpO_2$, is reported as a percentage every second by the pulse oximeter. Normal oxygen saturation levels range between 90 and 95%.

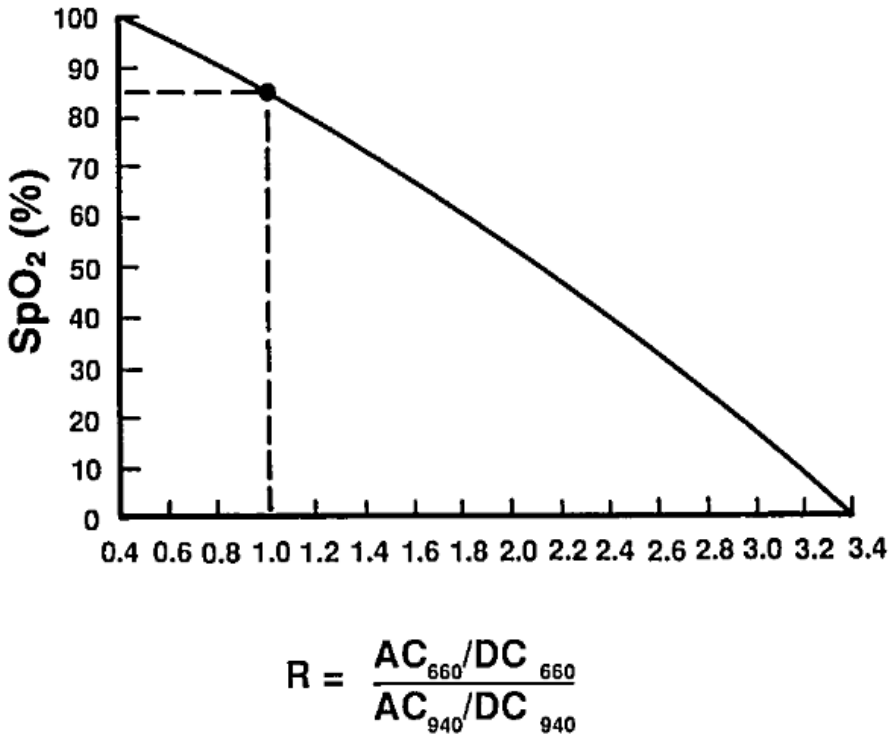

Figure 1-4: Typical pulse oximeter calibration curve, illustrating the relationship between the measured ratio of fractional changes in light intensity at two wavelenths, R, and estimated oxygen saturation $\%SpO_2$. Adapted from Figure 4 in [27].

1.2.2 Waveform Morphology

The photoplethysmogram waveform is similar in shape to the arterial blood pressure waveform, but has several morphological differences which prevent simple use of the $wSQI$ and $jSQI$ algorithms on PPG. As noted earlier, the PPG and ABP waveforms have different scales, and the amplitude of PPG waveform typically ranges from 0 to 1 rather than from 30 to 300 mmHg. There is no direct meaning for low or large pulse amplitudes in the PPG waveform. The PPG amplitude can be modulated by respiratory activity, as with the ABP. In processed waveforms, the amplitude is somewhat arbitrary due to automatic gain controls by the electronic monitor. The variability in pulse-to-pulse time follows the activity of the heart. When the signal is of good quality, the PPG pulse ampliutude varies closely with the stroke volume of the heart on a beat-by-beat basis, and with respiration (through respiratory sinus arrhythmia) [17]. The onset of each PPG pulse follows the onset of the QRS complex in the electrocardiogram and the onset of the corresponding pulse in radially-measured ABP. This can be quantified by the pulse transit time (PTT), which is computed as

$$PTT = t_{PPO} - t_{ecgQRS}, \tag{1.6}$$

where t_{PPO} is the PPG pulse onset time and t_{ecgQRS} is the onset time of the corresponding QRS complex in the electrocardiogram, which should occur between the current and last PPG pulse [5].

1.2.3 Artifacts

There are several limitations to the accuracy of pulse oximetry, including attenuation due to poor perfusion, skin pigmentation, and nail polish [24]. Inaccurate oxygen saturation values in certain types of anemic patients are due to modified hemoglobin which cannot be characterized by the normal hemoglobin light absorption spectrum. Artifacts due to ambient gas or fluorescent lighting have also been of concern, especially for those oscillating frequencies which are near the harmonic frequencies of the pulse oximeter's LED pulsations [24]. The waveform is subject to arbitrary baseline

shifts and to sudden amplitude changes due to the monitor's automatic gain control. Noise in the signal may cause the amplitude of the PPG waveform to saturate at a maximum or minimum value, or to rest at some random fixed value. However, the artifacts of largest concern are caused by motion of the sensor relative to the skin (generally due to patient movement) [12, 25, 22].

Researchers have investigated several methods for PPG artifact reduction, which can be categorized into three types of approach: stationary filtering based on frequency content [12], adaptive filtering based on energy changes in the waveform [4, 30], and adaptive filtering based upon data from an external sensor [25, 7, 28, 29]. Hayes *et al.* used spectral analysis to determine the motion artifact frequency range to be greater than three times the PPG fundamental frequency (heart rate); signal quality was then quantified by taking the proportion of artifact signal power to total signal power [12]. Coetzee *et al.* used recursive-least-squares adaptive filtering of patient waveforms with a synthetic reference signal to reduce noise and reconstruct waveforms [4]. Once artifacts have been identified, Kalman filters can be used to extract autoregressive coefficients for interpolation and smoothing of noisy pulse wave segments [30]. The performance of this method depends on the order of the autoregressive model. Sokwoo *et al.* have characterized motion artifacts by designing a snug-fitting ring sensor equipped with an accelerometer for fingerbase PPG measurements [25]. Adaptive filtering based on Laguerre models has been used to characterize the relationship between the PPG waveform and acceleration of the hand and finger, and to remove PPG motion artifacts [7, 28, 29]. Identification of PPG segments with poor signal quality attributed to motion artifact has been achieved by comparing the pulse rate obtained from the PPG waveform to the ECG-derived heart rate [22]. Gil *et al.* used Hjorth parameters to estimate the dominant frequency and spectral bandwidth of PPG waveforms measured from pediatric patients while in sleep, and applied thresholds to mark regions of gross artifact [8, 9]. However, few others have used these artifact reduction techniques to identify artifact types and create signal quality measures. None have studied PPG signal quality in the context of adult ICU patients, or under conditions of arrhythmias. We believe the stationary and adaptive

filtering approaches can be combined for more robust artifact detection.

1.3 Overview of Thesis

The goal of this thesis is to improve performance of ICU bedside monitors by suppression of false critical ECG arrhythmia alarms through the use of information derrived from simultaneously acquired PPG and ABP waveforms. Augmentation of the false alarm suppression framework presented by Clifford *et al.* [1, 3] to employ the PPG waveform requires both feature extraction and signal quality assessment. Two algorithms have been created for this purpose. Chapter 2 introduces the $pSQI$ algorithm, which employs spectral analysis to detect large artifacts for PPG signal quality assessment. Chapter 3 introduces the $aPPG$ algorithm, which employs time-series analysis to detect PPG pulse onsets. The results of these two algorithms are incorporated into a new false alarm suppression framework, which is described in Chapter 4. Evaluation of these methods and a discussion of improvements can be found in Chapter 5, as well as a discussion of future research efforts.

THIS PAGE INTENTIONALLY LEFT BLANK

Chapter 2

Signal Quality Assessment

The use of the photoplethysmogram waveform for electrocardiogram alarm corroboration requires a guarantee of the absence of artifact in the PPG waveform. Signal quality assessment is therefore a necessary component of the false alarm suppression framework.

2.1 Previous Work

Our PPG signal quality assessment is based on the identification of artifact periods using spectral power characteristics, as performed by Gil *et al.* [8, 9]. Sörnmo *et al.* estimated the dominant frequency and half-bandwidth of the spectral distribution of the waveform using Hjorth parameters [13, 14]. Gil *et al.* thresholded these parameter values to identiify periods of major artifact.

The Hjorth parameters characterize a time signal in terms of its amplitude, time scale, and complexity. The parameters of a discrete signal, $x[n]$, where n is the sample number, are derived from the moments of the power spectrum $S_x(e^{j\omega})$, where ω is the frequency in radians [13, 14]. The ith-order spectral moment is defined as

$$\bar{\omega}_i = \int_{-\pi}^{\pi} \omega^i S_x(e^{j\omega}) d\omega. \tag{2.1}$$

Since the power spectrum is symmetric about the $\omega = 0$ frequency axis, the odd

moments are all zero. However, the even moments can be used to estimate the shape of the power spectrum of the signal.

We assume that the signal $x[n]$ is a sampled version of a continuous time signal $x_c(t)$ with sampling period T_s, such that $x[n] = x_c(nT_s)$ for $n = 0, 1, \ldots, N-1$. The spectral moments can be computed from the mean power of $x_c(t)$ and its derivatives,

$$\bar{\omega}_0 = \int_{-\pi}^{\pi} S_x(e^{j\omega}) d\omega = 2\pi E[{x_c}^2(t)], \tag{2.2}$$

$$\bar{\omega}_2 = \int_{-\pi}^{\pi} \omega^2 S_x(e^{j\omega}) d\omega = 2\pi {T_s}^2 E\left[\left(\frac{dx_c(t)}{dt}\right)^2\right], \tag{2.3}$$

$$\bar{\omega}_4 = \int_{-\pi}^{\pi} \omega^4 S_x(e^{j\omega}) d\omega = 2\pi {T_s}^4 E\left[\left(\frac{d^2x_c(t)}{dt^2}\right)^2\right], \tag{2.4}$$

where $E[y]$ indicates the calculation of the expectation of the argument, y. Note that the zeroth moment corresponds to the variance, σ_a^2, of the amplitude of the zero-mean signal $x[n]$. Similarly, the second moment corresponds to the variance, σ_d^2, of the slope values of the signal, and the fourth moment corresponds to the variance, σ_{dd}^2, of the rate of change of slope in the signal.

The first Hjorth parameter (termed *activity*),

$$H_0 = \bar{\omega}_0, \tag{2.5}$$

gives a measure of mean signal power. The second Hjorth parameter (termed *mobility*) is defined as

$$H_1 = \sqrt{\frac{\bar{\omega}_2}{\bar{\omega}_0}}. \tag{2.6}$$

From a time-domain perspective, H_1 gives a measure of the standard deviation of the slope of $x[n]$ relative to the standard deviation of the amplitude. As a power ratio, this parameter becomes a measure of frequency variance of the power spectral density. The third Hjorth parameter (termed *complexity*) is expressed as

$$H_2 = \sqrt{\frac{\bar{\omega}_4}{\bar{\omega}_2} - \frac{\bar{\omega}_2}{\bar{\omega}_0}}. \tag{2.7}$$

The first term in the difference can be interpreted as the mobility or frequency variance of the power spectral density of the first derivative of $x[n]$, where the signal power has been redistributed to the higher frequencies. The complexity parameter therefore represents the difference between the frequency variance of the first derivative and the frequency variance of the original signal. In the time domain, this parameter can be interpreted as the variance of the curvature values during one period with respect to the variance of the slope values during that period. A rapidly varying signal with complex morphology, such as high-frequency noise, will exhibit more variance in the curvature of the signal than a smoothly-varying signal such as a sinusoid.

Hjorth parameters can be efficiently computed in the time domain because the spectral moments can be computed from the first and second derivatives of the time series [13]. For discrete signals, these derivates are approximated by the first and second difference equations, such that

$$x^{(1)}[n] = x[n] - x[n-1], \tag{2.8}$$

$$x^{(2)}[n] = x[n+1] - 2x[n] + x[n-1], \tag{2.9}$$

where

$$\frac{d^i x_c(t)}{dt^i} \approx \frac{x^{(i)}[n]}{{T_s}^i}. \tag{2.10}$$

The interpretation and use of the Hjorth parameters for spectral estimation can be clarified through an example. Suppose the input signal is a pure sinusoid with fundamental frequency 1 Hz. The power spectrum of this signal consists of two impulses centered at the positive and negative fundamental frequency of the sinusoid. The slopes of the input signal are taken from the first derivative of the signal, which is the cosine function. The variance of the slope values generated over one period

with respect to the amplitude of the signal during that period is expressed by the mobility parameter, which should equal 1 for this signal because the variance of the sine and cosine values is the same. From a frequency perspective, the mobility parameter describes the frequency of the signal. (The mobility will be greater than 1 for sinusoids of higher frequencies, and less than 1 for sinusoids of lower frequencies, due to scaling of the signal amplitude when a derivative is taken.) If the the signal is a pure sinusoid, the complexity parameter should equal zero, because the second derivative of the signal carries the same fundamental frequency as the first derivative and the signal itself. The mobility of the first derivative is also 1, and because the complexity parameter describes the difference between the frequency variance of the first derivative and the frequency variance of the original signal, the complexity parameter equals zero.

Because the Hjorth parameters are based on the concept of variance, they also exhibit the additive properties of variance [13]. For example, in the case where the signal $x[n]$ represents a superposition of sinusoids, the mobility parameter will provide some weighted measurement of all the present fundamental frequencies. If the signal is periodic but not purely sinusoidal, the power spectrum will exhibit a peak associated with the main frequency of the signal but will also have non-zero bandwidth. The mobility parameter, as the frequency variance of the power spectrum, will not represent this main frequency, and the complexity parameter will have a non-zero value, reflecting the extent to which the morphology of the signal deviates from that of a sinusoid.

In the analysis of physiologic signals such as the PPG waveform, the input signal is periodic but near-sinusoidal. This means the power spectrum has a resonant frequency related to the heart rate, and has some non-zero bandwidth. Gil *et al.* [8, 9] used the mobility parameter, H_1, to estimate the dominant frequency of the signal, and used the complexity parameter, H_2, to estimate the half-bandwidth of the PPG power spectrum. The H_1 value does not provide an accurate estimate of dominant frequency or heart rate, as is illustrated in Figure 2-1. However, waveforms with physiologically normal morphology and heart rate should exhibit power spectral

densities with most of their mass within a certain range.

Gil, Vergara, and Laguna [9] describe a PPG artifact detector which employs mobility and complexity of the PPG waveforms. At each sample, H_1 and H_2 were determined from estimates of the moments of a P-sample window of PPG data:

$$\hat{\bar{\omega}}_i[n] \approx \frac{2\pi}{P} \sum_{k=n-(P-1)}^{n} (x^{(i/2)}[k])^2, \qquad i = 0, 2, 4 \tag{2.11}$$

where $x^{(i/2)}[k]$ is the $i/2$ derivative of $x[k]$.

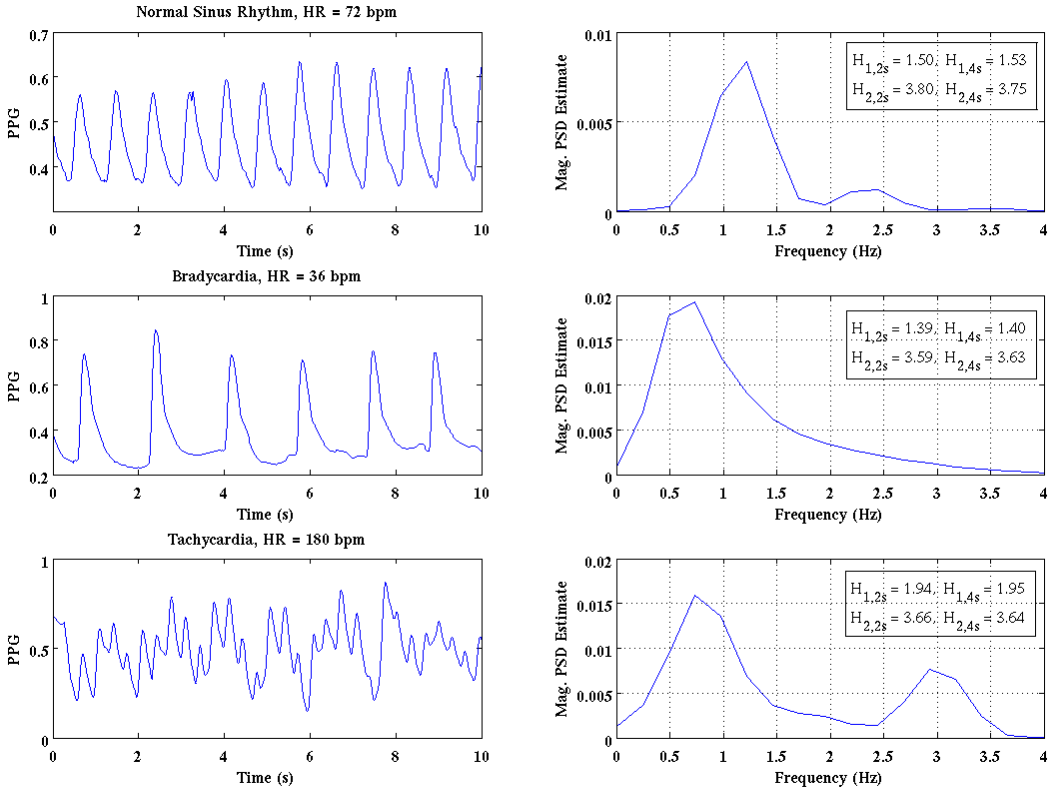

Figure 2-1: Hjorth parameter calculations for PPG segments at various heart rates. Printed with each power spectrum is the mean of the H_1 and H_2 Hjorth parameters, which were calculated using non-overlapping 2s and 4s windows from the zeroth, second, and fourth moments of the power spectrum of the PPG waveform according to Equation 2.11.

In their study of PPG data from 26 children, Gil *et al.* [8, 9] found that the PPG signal is of high quality when mobility (H_1) lies within a range whose upper threshold

is specified by ${\eta_1}^u$ and whose lower threshold is given by ${\eta_1}^l$. The signal is considered to be of good quality when complexity (H_2) lies below a threshold, η_2. Conversely, artifactual regions are portions of the signal where the dominant frequency differs too much from the heart rate, $H_1 < {\eta_1}^l$ or $H_1 > {\eta_1}^u$, or where the power spectrum is too wide, $H_2 > \eta_2$.

The thresholds used to detect artifact, ${\eta_1}^l$, ${\eta_1}^u$, and η_2 are set at a static value relative to $\tilde{H_1}$ and $\tilde{H_2}$, the medians of the H_1 and H_2 values, which are computed over the entire length of the provided data:

$${\eta_1}^l = \alpha_1 + \tilde{H_1}, \tag{2.12}$$

$${\eta_1}^u = \alpha_2 + \tilde{H_1}, \tag{2.13}$$

$$\eta_2 = \alpha_3 + \tilde{H_2}. \tag{2.14}$$

In the work of Gil *et al.*, $\alpha_1 = -1$, $\alpha_2 = 1.4$, and $\alpha_3 = 3$.

A single recording of data provided to the algorithm could be minutes long, or it could be hours long. This method for setting thresholds thus assumes that the majority of the recording contains signal with no artifact, and the heart rate and rhythm are normal and stable. If the heart rate varies significantly over the interval, portions of the segment may get marked as artifact even if the signal is of high quality. Furthermore, the thresholds have been chosen based on data from pediatric patients while in sleep, where motion artifacts are less likely to appear. The threshold settings for artifact determination therefore may not hold for adult ICU patients, which are the focus of this study.

2.2 Modifications for Prototype Artifact Detector

We have implemented the artifact detection algorithm of Gil *et al.* [8, 9], which we will refer to as *pSQI*, on PPG data from the MIMIC I [20] and MIMIC II [23] databases.

This prototype system was used to provide a rough estimate of the total amount of good quality PPG data available for use, as well as to screen for good quality PPG segments while testing the $aPPG$ pulse onset detection algorithm, described in Chapter 3.

We have created a binary signal quality index, SQI, that takes value 0 for artifactual segments, and takes value 1 for good-quality segments. An illustration of the performance of the artifact detector is shown in Figure 2-2 on page 34. Note that for the temporal window over which H_1 and H_2 are calculated, Gil *et al* use a window size of 5 seconds, and we use non-overlapping windows of length 2 seconds. The choice of 2 seconds is to provide the shortest temporal window possible which would capture at least one pulse at 30 beats per minute or faster. When the SQI value drops from 1 to 0, indicating artifact, it does so at the back (earliest) edge of the P-sample window. The SQI steps from 0 to 1 at the leading (latest) edge of the window. In other words, the output of the SQI detector takes a safe harbor approach and labels any section that may contain some artifact as artifactual, even though there may be some good quality data near the start and/or end of the window. Furthermore, if two artifactual segments are not separated by more than 5 seconds of clean data, they are fused into one longer artifactual period. Therefore regions with SQI equal to 1 are unlikely to have artifactual data in them, even at the region's edges.

The prototype system has three main limitations. First, the thresholding mechanism is not adaptive, and assumes that the majority of a record contains clean data, since the thresholds are set relative to the mean Hjorth parameter values across all the segments in a record. Secondly, the thresholds were determined from data recorded in a pediatric sleep study and should not be applied to adult ICU patient data without further investigation. The age, activity, condition, and treatment of adult ICU patients differs systematically from sleeping pediatric patients. Third and most importantly, while regions of normal sinus rhythm and normal pulse morphology are marked as having high PPG quality, periods of high PPG signal quality (i.e. clearly discernable beats despite low amplitude or atypical morphology) recorded when the patient was suffering from a cardiac arrhythmia are often marked as artifact. Specif-

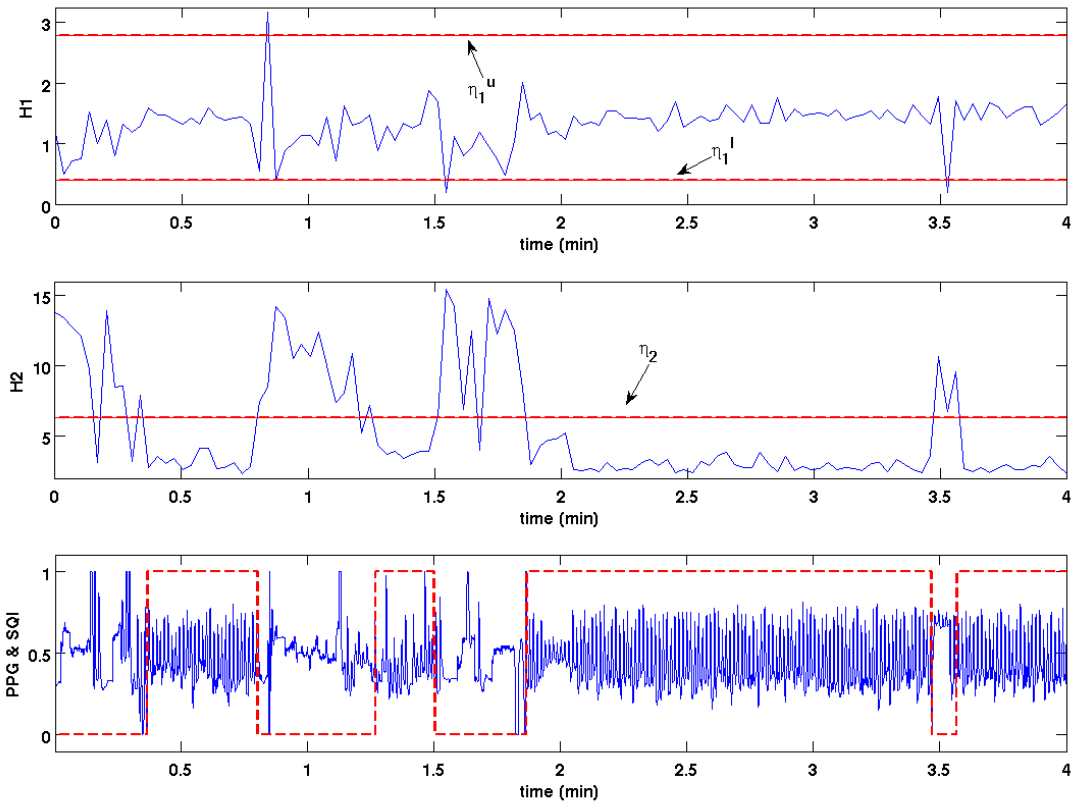

Figure 2-2: PPG artifact detection based on Hjorth parameters, as described in [9] on MIMIC II patient record $a44545$. Non-overlapping window size = 2 s. (a) Mobility, $H_1[n]$ (see Eqn. 2.6), with thresholds ${\eta_1}^l$ and ${\eta_1}^u$, outside of which the signal is considered artifactual. (b) Complexity, $H_2[n]$ (see Eqn. 2.7), with spectral width threshold η_2, above which the signal is considered artifactual. (c) PPG waveform (solid line) and signal quality (dashed line). The PPG waveform exhibits good quality when ${\eta_1}^l < H_1 < {\eta_1}^u$ and $H_2 < \eta_2$.

ically, the prototypical *pSQI* algorithm marks periods of PPG with low heart rates as artifact, thereby ignoring high quality signals measured during periods of bradycardia. We address these limitations by examining the H_1 and H_2 parameter values in adult ICU patient data in the case of normal sinus rhythm and under various arrhythmia conditions.

2.3 Adaptive Assessment of Signal quality

Our goal is to suppress false arrhythmia alarms in the ECG signals of ICU beside monitors by consulting information in simultaneously recorded PPG signals. To do this, we require a trust metric for the PPG waveform. By employing the Hjorth parameters to analyze the PPG waveform recorded before an alarm, we can determine if the PPG is of high enough quality to provide a reliable estimate of heart rate. Due to the limitations discussed in the previous section, it is important to assess PPG signal quality in the context of the specific arrhythmia alarm type which has been generated by the monitor. Thus we examine the H_1 and H_2 Hjorth parameter values computed from the PPG waveform segments recorded just before true and false arrhythmia alarms are issued. Hjorth parameter thresholds must be determined for each arrhythmia alarm type, since spectral content differs based on heart rate.

2.3.1 Structure and Availability of Waveform Data

For this research, the ICU photoplethysmogram waveforms are taken from the MIMIC II database [23]. Through this database we have access to approximately synchronous waveforms with combinations of respiration, electrocardiogram, arterial blood pressure, and photoplethysmogram waveforms, sampled at 125 Hz, recorded by Phillips CMS bedside patient monitors (Phillips Medical Systems, Andover, MA). The data is organized by patient records, which also contain annotations of all ECG-, ABP-, and PPG-issued alarms.

Each patient record (which contains data from an individual ICU visit) may be broken into several record segments of variable length. A new segment begins when-

ever the number or type of channels of data changes, the gain of any channel of data changes, the waveform file becomes corrupt, the time stamps become non-contiguous (due to network errors), or the data collection unit is stopped for a few minutes to allow changing of disks. The types of waveforms in one segment of the record may not necessarily be present in a different segment of the same record. A total of $20,931$ segments of varying lengths from $2,997$ patient records are accessible. Only 618 of these records contain electrocardiograms which triggered critical (life-threatening) ECG arrhythmia alarms, with $6,977$ critical alarms total.

We have categorized each waveform segment based upon its signal content, and created groups for segments containing ECG, ABP, PPG, and waveforms labeled "unknown." Inspection of these waveforms shows they are mostly mislabeled PPG waveforms, so in estimating the amount of available photoplethysmogram data, we take the union of the set of segments containing labeled PPG waveforms with the set of segments containing a waveform labeled "unknown." The number of hours of available waveforms from these records for training and testing the signal quality algorithm and ECG false alarm suppression algorithm is summarized in Table 2.1 and illustrated in Figure 2-3. There are at least $47,581$ hours of simultaneous PPG and ECG data available for training and testing the signal quality algorithm and ECG false alarm suppression algorithm. If $50,520$ represents the total hours of all the patient stays, then pulse oximeter data is available 94% of the time. (Note that there are only $17,833$ hours of simultaneous ECG and ABP waveforms, representing ABP availability during only 35% of the patient record hours. This is much less than that available from the PPG). However, when we add the criterion that life-threatening arrhythmia alarms must be present at some point in the record, we reduce the number of cases by 18% and available hours of waveform data by 35%. Approximately $11,231$ hours of simultaneous ECG, ABP, PPG from 272 cases are available for training and testing the PPG pulse onset detector and to evaluate performance of a PPG-enhanced false alarm suppression framework. After requiring that the record is longer than 5 minutes, contains critical arrhythmia (asystole, extreme bradycardia, extreme tachycardia, ventricular tachycardia, or ventricular fibrillation/tachycardia) alarms,

Table 2.1: Estimated hours of available waveform data

Waveforms	All Available Records		Records with Alarms	
	No. Cases	No. Hours (%)	No. Cases	No. Hours (%)
ECG	756	50,520 (100%)	618	32,897 (65%)
ECG & PPG	728	47,581 (94%)	596	31,325 (62%)
ECG & ABP	315	17,833 (35%)	283	11,885 (24%)
ECG & ABP & PPG	303	16,654 (33%)	272	11,231 (22%)

and is not the record of a patient with an intra-aortic balloon pump, the final number of cases considered is 181.

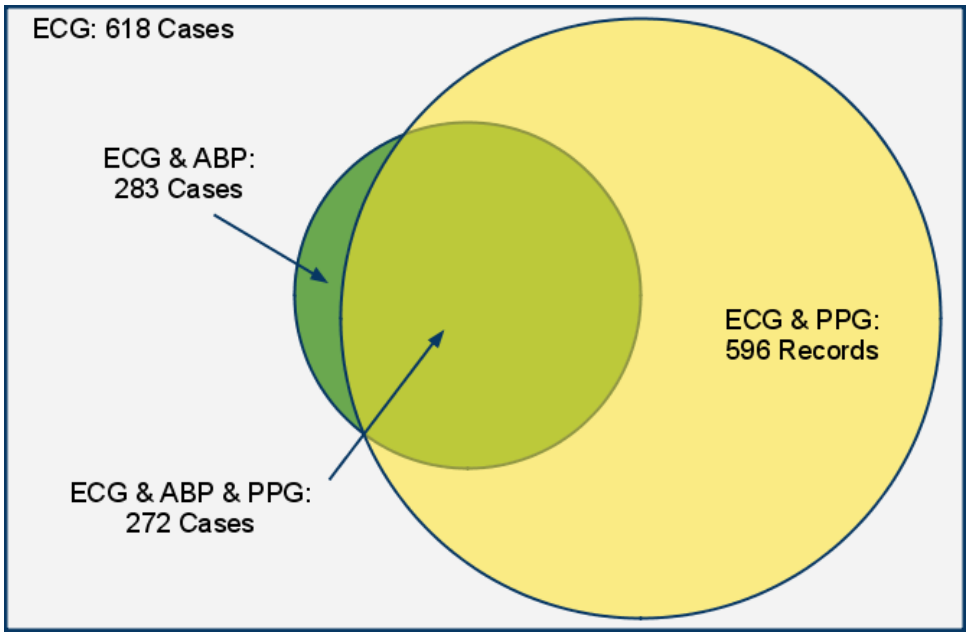

Figure 2-3: Waveform data available with critical electrocardiogram alarms. Of the 618 cases with critical ECG alarms, 272 cases have simultaneously recorded ECG, ABP, and PPG waveforms.

2.3.2 Preparation of Alarm Data

From the MIMIC II database, ICU patients have been selected whose records include simultaneously recorded ECG, ABP, and PPG waveforms and some number of life-threatening cardiac arrhythmia alarms, namely asystole, extreme bradycardia, extreme tachycardia, ventricular tachycardia, and ventricular fibrillation. Each of these alarms were annotated independently as True, False, or Indeterminable by one signal

processing expert with over a decade of experience in analyzing such data and one graduate student with graduate level training in cardiac electrophysiology [18, 11]. One physician with several decades of electrocardiographic interpretation experience adjudicated the annotations. The annotations and adjudications were made by reviewing all ECG, ABP, and PPG waveforms surrounding each alarm onset over any length of window size desired (but generally 30 seconds) using open-source waveform viewing software ('WAVE', available at PhysioNet.org [19]). Patients with intra-aortic balloon pumps were excluded from this study. The final "gold standard" annotated alarm set included a total of $4,012$ alarms from 181 ICU patients.

The alarm category of ventricular fibrillation/tachycardia yielded no true ventricular fibrillation annotations, where the ECG waveform accompanying the alarm exhibited uncoordinated ventricular contraction and the ABP and/or PPG showed no pulsatile activity until the patient received a defibrillating shock. The alarm was always triggered under circumstances of rapid ventricular tachycardia, which usually degenerates into ventricular fibrillation. These ventricular fibrillation/tachycardia alarms were therefore annotated in the same manner as ventricular tachycardia alarms and were combined with alarms from the ventricular tachycardia category. That is, if ventricular fibrillation was not present, but ventricular tachycardia was, the alarm was marked as true. Similarly, if the associated waveforms demonstrated neither ventricular fibrillation nor ventricular tachycardia, the ventricular fibrillation/tachycardia alarm was annotated as false.

A separate signal quality study was conducted for each of the alarm types. Patients exhibiting the alarm in question were ranked by the number of alarms in the record and sorted into training and test sets. Each set had an equal number of patients and roughly equal number of alarms. The number of patient records and the relative frequency of true and false alarms of each type in the training and testing sets are detailed in Tables 2.2, 2.3, and 2.4. Compared to the data set in the study performed by Aboukhalil *et al.* [1], our data set has a higher percentage of ventricular tachycardia alarms, and fewer extreme bradycardia and extreme tachycardia alarms. The false alarm rates in our data set are similar, except for extreme tachycardia alarms, which

Table 2.2: Annotated critical ECG arrhythmia alarms in gold standard database. For example, there are 29 true asystole alarms, indicating that 1.2% of all alarms in the database are true asystole alarms, and that 7.8% of all asystole alarms in the data set are true.

Alarm Type	No. Patients	No. Alarms		
		All (% All)	True (% All) (% Type)	False (% All) (% Type)
Asystole	95	639 (15.9)	50 (1.2) (7.8)	589 (14.7) (92.2)
Extreme Bradycardia	49	282 (7.0)	174 (4.3) (61.7)	108 (2.7) (38.3)
Extreme Tachycardia	66	832 (20.7)	762 (19.0) (91.6)	70 (1.7) (8.4)
Ventricular Tachycardia	146	2259 (56.3)	1194 (29.7) (52.7)	1068 (26.6) (47.3)
Total (Averages)	181	4012	2177 (13.6) (53.5)	1835 (11.4) (46.6)

appear less frequently in our alarm collection.

2.3.3 Preparation of Normal Sinus Rhythm Data

To provide an understanding of the spectral distributions of PPG signals during sinus rhythm, and to provide a set of data for training a pulse onset detection algorithm, we identified a large amount of clean PPG data recorded during sinus rhythm.

From the MIMIC II database, 748 half-minute segments of non-artifactual PPG signals exhibiting normal sinus rhythm were screened for high signal quality using the prototype $pSQI$ algorithm and examined by eye to ensure the lack of gross artifact, signal dropout, and indications of arrhythmia. Beat onsets were detected (using a pulse onset detection algorithm described in Chapter 3), and a vector of beat-by-beat instantaneous heart rates was formed for each PPG segment. Those segments which exhibited mean instantaneous heart rates between 60 and 85 beats per minute, with a standard deviation less than 5 beats per minute, were retained to yield 264 half-minute epochs from 43 patients. The H_1 and H_2 parameters for each non-overlapping 2 s window of these epochs were recorded.

Table 2.3: Annotated critical ECG arrhythmia alarms in Training Set. For example, in the training set there are 29 true asystole alarms, indicating that 1.3% of all alarms in the training set are true asystole alarms, and that 8.3% of all asystole alarms in the training set are true.

Alarm Type	No. Patients	No. Alarms		
		All (% All)	True (% All) (% Type)	False (% All) (% Type)
Asystole	48	349 (15.3)	29 (1.3) (8.3)	320 (14.0) (91.7)
Extreme Bradycardia	25	205 (9.0)	131 (5.7) (63.9)	74 (3.2) (36.1)
Extreme Tachycardia	33	519 (22.7)	498 (21.8) (95.9)	21 (0.9) (4.1)
Ventricular Tachycardia	73	1213 (53.1)	711 (31.1) (58.6)	502 (22.0) (41.4)
Total (Averages)	127	2286	1369 (15.0) (56.7)	917 (10.0) (43.3)

Table 2.4: Annotated critical ECG arrhythmia alarms in Test Set. For example, in the test set there are 21 true asystole alarms, indicating that 1.2% of all alarms in the test set are true asystole alarms, and that 7.2% of all asystole alarms in the test set are true.

Alarm Type	No. Patients	No. Alarms		
		All (% All)	True (% All) (% Type)	False (% All) (% Type)
Asystole	47	290 (16.8)	21 (1.2) (7.2)	269 (15.6) (92.8)
Extreme Bradycardia	24	77 (4.5)	43 (2.5) (55.8)	34 (2.0) (44.2)
Extreme Tachycardia	33	313 (18.1)	264 (15.3) (84.3)	49 (2.8) (15.7)
Ventricular Tachycardia	73	1046 (60.6)	480 (27.8) (45.9)	566 (32.8) (54.1)
Total (Averages)	126	1726	808 (11.7) (48.3)	918 (13.3) (51.7)

2.3.4 Hjorth Parameter Assessment By Alarm Type

For each alarm in the training set, thirty seconds of PPG data prior to the alarm were extracted and analyzed to compute the H_1 and H_2 parameters over 2 s non-overlapping windows. The Hjorth parameters were then sorted by associated alarm type and condition (the veracity of the alarm, true or false). Distributions of these H_1 and H_2 values are illustrated using box and whisker plots in Figures 2-4 and 2-5.

The mobility parameter (H_1) estimates the dominant frequency of the PPG signal, which is noticeably lower in the case of true bradycardia alarms compared to waveforms at normal sinus rhythm or faster heart rates. False bradycardia alarms are accompanied by waveforms with the dominant frequency in the same range as those exhibiting normal or fast heart rates. True asystole alarms are accompanied by a wide range of dominant frequencies, indicating the high prevalence of noise and gross artifact, or missing signal on the PPG channel, while PPG waveforms measured during false asystole alarms exhibit a dominant frequency in the range of normal and fast heart rates.

The complexity parameter (H_2) shows more promise for distinguishing between high signal quality PPG waveforms in true and false conditions of extreme tachycardia or ventricular tachycardia alarms. For the ventricular tachycardia category, PPG waveforms accompanying true alarms exhibit more "band-limited" power spectra than those alongside false alarms. Once again, the wide range of complexity parameters for true asystole alarms indicates wider bandwidth, which is associated with a flat, DC-like signal.

A two-sample Kolmogorov-Smirnov test was performed between the true and false distributions for each alarm condition and both Hjorth parameters. The results are presented in Table 2.5. The H_1 distributions for extreme tachycardia alarms were not significantly different. In every other case, the distributions were found to be significantly different ($p < 0.0001$).

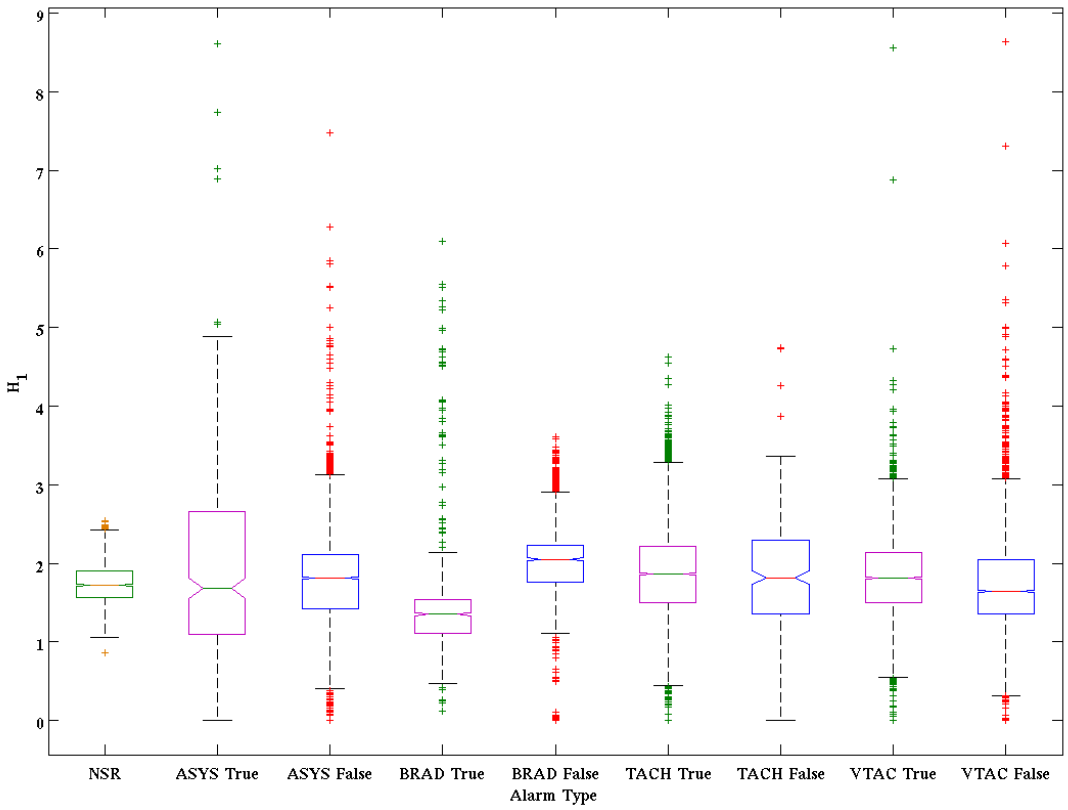

Figure 2-4: Box and whisker plot of mobility parameter (H_1) distributions by alarm type and condition (veracity). ASYS = asystole; BRAD = extreme bradycardia; TACH = extreme tachycardia; VTAC = ventricular tachycardia.

2.3.5 Threshold Setting

As a first pass, we assume that most of the "mass" in the distributions of the H_1 and H_2 parameters under true alarm conditions is calculated from clean PPG waveforms. These segments most likely contributed to the annotation of the alarm as true. We therefore use values of H_1 and H_2 which are at the edges of the distributions to indicate poor signal quality.

In the remainder of this study, we examined 512 combinations of the Hjorth parameter thresholds, ${\eta_1}^l$, ${\eta_1}^u$, and η_2. For each threshold we chose eight values spanning the upper and lower interquartile ranges in the true alarm distributions. For ${\eta_1}^l$, we chose eight uniformly spaced values between one and a half interquartile ranges below the lower quartile and the median value of each true alarm H_1 distribution. For ${\eta_1}^u$,

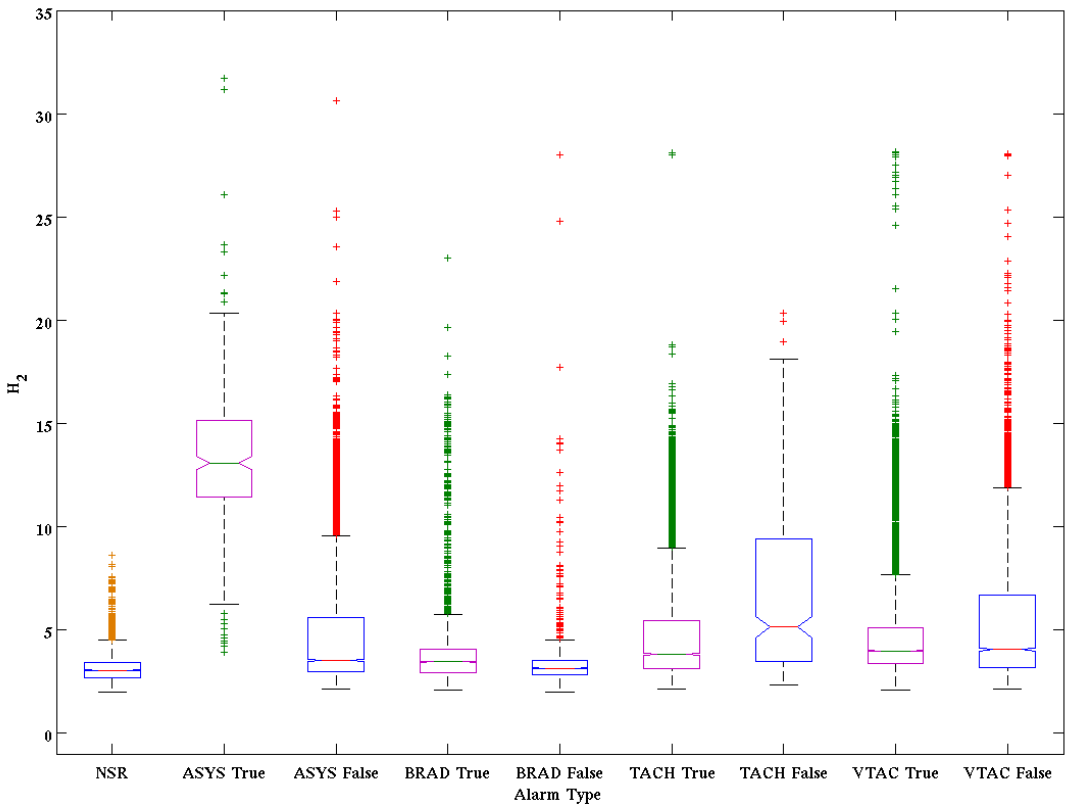

Figure 2-5: Box and whisker plot of complexity parameter (H_2) distributions by alarm type and condition (veracity). ASYS = asystole; BRAD = extreme bradycardia; TACH = extreme tachycardia; VTAC = ventricular tachycardia.

we chose eight uniformly spaced values between the median value and one and a half interquartile ranges above the upper quartile of each true alarm H_1 distribution. For η_2, we chose eight uniformly spaced values between the median value and one and a half interquartile ranges above the upper quartile of each true alarm H_2 distribution. The threshold ranges tested are summarized in Table 2.6, where each range is distributed from the lower value to the upper value in eight equal increments. Each of these 512 Hjorth parameter thresholds was used in the false alarm suppression framework described in Chapter 4, and the thresholds which yielded the best false alarm suppression rate on the training set was chosen for use in the algorithm.

Table 2.5: Results of Kolmogorov-Smirnov tests for H_1 and H_2 during true and false alarms to be sampled from different distributions

Alarm Type	H_1 significance	H_2 significance
Asystole	$p < 0.0001$	$p < 0.0001$
Extreme Bradycardia	$p < 0.0001$	$p < 0.0001$
Extreme Tachycardia	$p = 0.01$	$p < 0.0001$
Ventricular Tachycardia	$p < 0.0001$	$p < 0.0001$

Table 2.6: Ranges of Hjorth parameter threshold settings tested for each alarm type

Alarm Type	Threshold Range		
	${\eta_1}^l$ range Increment	${\eta_1}^u$ range Increment	η_2 range Increment
Asystole	$[0 \ldots 1.68]$ 0.24	$[1.68 \ldots 4.96]$ 0.47	$[13.1 \ldots 20.6]$ 1.1
Extreme Bradycardia	$[0.493 \ldots 1.35]$ 0.12	$[1.35 \ldots 2.17]$ 0.12	$[2.39 \ldots 5.79]$ 0.49
Extreme Tachycardia	$[0.443 \ldots 1.87]$ 0.20	$[1.87 \ldots 3.29]$ 0.20	$[3.83 \ldots 8.99]$ 0.74
Ventricular Tachycardia	$[0.555 \ldots 1.81]$ 0.18	$[1.81 \ldots 3.08]$ 0.18	$[3.98 \ldots 7.70]$ 0.53

2.4 Use of *pSQI*

The *pSQI* algorithm is used in a false alarm suppression framework to assess the signal quality in the PPG waveform just preceding an ECG arrhythmia alarm. If the signal quality is high, the PPG waveform exhibits spectral characteristics of the cardiac arrhythmia in question, and we trust the heart rate estimated from that segment. Additional logic can then be used to accept or suppress the issued alarm, as in the works of Aboukhalil, Clifford, *et al.* [1, 3].

Chapter 3

PPG Pulse Onset Detection

In order to perform heart rate estimation and beat-by-beat extraction of PPG waveform features, the duration of each pulse must be determined. This can be achieved by pulse onset detection, assuming the pulse lasts from one onset to the next, and no beats are missed or erroneously detected.

3.1 Previous Work

For the simple purpose of heart rate estimation from the photoplethysmogram waveform, peak detection is a simple and effective method for pulse identification. Pulse peak detection can be made robust to noise and movement artifacts if adequate filtering and thresholding is applied, as demonstrated by Yu *et. al* [31]. However, studies of irregular pulse morphology or rhythms require feature analysis on the whole pulse. Detection of pulse onsets allows for pulse extraction and study of irregular pulse morphology, as well as analysis of pulse transit time.

Zong *et al.* [32] have previously created the $wABP$ algorithm to detect the onset of arterial blood pressure pulses. Their algorithm passes the input blood pressure waveform,x_n, through a low-pass filter, then computes a slope sum function (SSF), which enhances the upslope of each pulse in the waveform. The low-pass filter is a second-order recursive filter with transfer function, frequency response, and difference equation given by Equations 3.1, 3.2 and 3.3.

$$H(z) = \frac{(1 - z^{-5})^2}{(1 - z^{-1})^2} \tag{3.1}$$

$$|H(\omega T)| = \frac{sin^2(3\omega T)}{sin^2(\omega T/2)} \tag{3.2}$$

$$y_n = 2y_{n-1} - y_{n-2} + x_n - 2x_{n-5} + x_{n-10} \tag{3.3}$$

For each time point, i, the SSF, z_i of the preceding w-sample window of the filtered signal, y_n , is computed as follows:

$$z_i = \sum_{k=i-n}^{i} \Delta u_k, \qquad \Delta u_k = \begin{cases} \Delta y_k, & \text{if } \Delta y_k > 0 \\ 0, & \text{if } \Delta y_k \leq 0 \end{cases} \tag{3.4}$$

where $1 + w \leq i \leq N$, N is the total number of samples in the ABP waveform, and $\Delta y_k = y_k - y_{k-1}$. The SSF is then passed through a decision rule to determine the occurrence of each pulse onset in the blood pressure waveform.

In the $wABP$ algorithm, the decision rule has two components, which we will refer to as the pulse initiation and pulse confirmation phases. In the pulse initiation phase, the algorithm determines that a pulse is initiated if the SSF value is greater than a threshold. The threshold is initialized by the average SSF value over the first 8 s of waveform data. To confirm that an ABP pulse with a strong upstroke is present, the difference between the maximum and minimum values of the SSF in a 150 ms window must exceed a static confirmation threshold. If both of these conditions are met, the pulse onset time is noted, and further detections are prohibited during the following 0.25 s refractory period. Adaptation of the threshold is achieved by lowering the initiation threshold by a constant value if 2.5 s have passed without any initiated detections, and by updating the initiation threshold according to the maximum SSF value of each detected pulse. The performance of the $wABP$ algorithm is illustrated in Fig. 3-1.

In Zong's original work [32], the $wABP$ algorithm was not evalutated in the presence of artifact or noise, and its performance was not evaluated during periods of arrhythmia, where the morphology of the blood pressure pulses deviates significantly

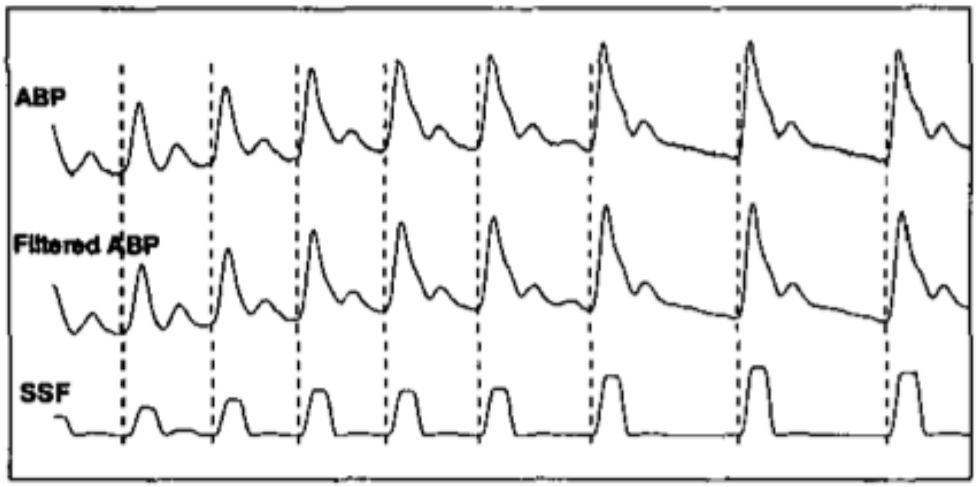

Figure 3-1: Use of the Slope Sum Function to detect pulse onsets in the arterial blood pressure waveform. Adapted from Figure 4 in [32].

from the morphology at normal sinus rhythm, and the algorithm is therefore expected to present unusual behavior. The $wABP$ algorithm contains no adaptations for heart rate variability. Furthermore, the limited adaptivity of the SSF pulse initialization threshold and the use of a static threshold on the range of the slope sum function indicates that the algorithm expects pulses of a certain amplitude and assumes there will be only small deviations in pulse pressure.

3.2 $aPPG$: Photoplethysmogram Pulse Onset Detection

The similarities between ABP and PPG pulse morphology prompted us to adapt the $wABP$ pulse onset detector for use on the photoplethysmogram waveform, which we will refer to as $aPPG$. As in the original $wABP$ algorithm, we have maintained a window size of 128 ms ($n = 16$ samples for a signal sampled at 125 Hz) for computing the SSF, which corresponds to the typical upslope duration of a PPG pulse under normal sinus rhythm heart rates. We have scaled and offset the PPG waveform input to resemble physiologic range for blood pressure measurements (in mmHg) in order to take advantage of the existing low-pass filter in $wABP$.

The amplitude of the PPG waveform can change for several reasons, including vasoconstriction, variation in pulse volume due to arrhythmia conditions, or as artifacts of automatic gain changes in the bedside monitors. Further modifications have therefore been made to allow $aPPG$ to perform robustly in the presence rapid amplitude changes.

The refractory period is set to 0.25 s by default, but is modified if provided with an estimate of the prior heart rate estimate, by assuming the length of the refractory period is 40% of the total pulse duration. For simplicity, we define pulse duration to be the pulse-to-pulse interval. This modification anticipates longer inter-pulse intervals during periods of true bradycardia or shorter inter-pulse intervals during periods of extreme tachycardia, by lengthening or reducing the refractory period (respectively) in the presence of a prior heart rate estimate.

To make the pulse detection algorithm robust to sudden gain changes in the PPG waveform, both the SSF pulse initiation and the SSF pulse confirmation phases of the decision rule have been made adaptive. As in $wABP$, the pulse initiation threshold is intialized to three times the average SSF value over the first 8 s of data. At each confirmed pulse onset detection, the threshold is adapted according to a fraction, T_c of the difference between the local maximum and minimum values of the SSF.

An appropriate change in slope in each PPG waveform pulse is determined using the magnitude of the corresponding SSF pulse. This SSF pulse confirmation threshold was set to a static value in $wABP$. However, a sudden decrease of the PPG signal gain proportionally decreases the slope of the PPG pulse onsets. The corresponding slope sum function peaks will also be diminished in magnitude. The static threshold developed for periods of higher PPG signal gain will miss these pulses of diminished amplitude. Therefore we adapt the pulse confirmation threshold. Adapting by the full amplitude of the SSF waveform results in missed detections when there is a sudden decrease in gain, so for a more robust system we adapt by $T_c = 70\%$ of the most recentltly detected SSF peak.

Two timer algorithms have been introduced, to adapt the respective thresholds independently. The first timer, also used in $wABP$, lowers the pulse initiation threshold

by a constant amount if no pulse has been initiated for more than 2.5 s. The second timer, new to $aPPG$, continuously decreases the pulse confirmation threshold by a fraction, $d_c = 0.1\%$ per time step (or 12.5% per second at 125 Hz), of the PPG waveform amplitude over the previous 5 s if no new pulse has been detected for more than four refractory periods. To avoid false pulse detections due to low-amplitude artifacts, a noise floor is set at half of the smallest expected true pulse amplitude. If the full possible range for the PPG waveform is 0 to 1, we expect the lowest pulse amplitude to be no smaller than 0.025, so we set the noise floor at 0.0125. The confirmation threshold is reset based on half of the PPG amplitude over the previous 5 s if the noise floor is reached.

The performance of the $aPPG$ algorithm is illustrated in Figures 3-2 and 3-3.

3.3 $aPPG$ Performance

To evaluate the performance of the prototype algorithm, we compared pulse onsets detected in the PPG waveform using $aPPG$ to a set of "chrome standard" beat annotations from the ECG and arterial blood pressure waveforms. That is, we chose locations where the ECG and ABP pulse detections agreed, and assumed a PPG pulse should also be present within a set period of time.

3.3.1 Data Acquisition, Pre-processing, and Evaluation Setup

Thirty one patient records of variable length containing simultaneously recorded ECG, ABP, and PPG signals are available the MIMIC I database [20]. Waveforms were extracted from all patient records, yielding $1,099.85$ hours of data total. The PPG waveforms were pre-processed to note the start and end points of any instance of flat-line artifact or signal dropout. The PPG waveforms were also screened for severe motion artifacts using a prototype $pSQI$ signal quality assessment scheme, described in Chapter 2 of this thesis. Any beats or blood pressure pulse onsets detected in segments of the record where the PPG had dropped out, was flat, or contained severe artifact (such as maximum or minimum saturations or high-frequency noise), were

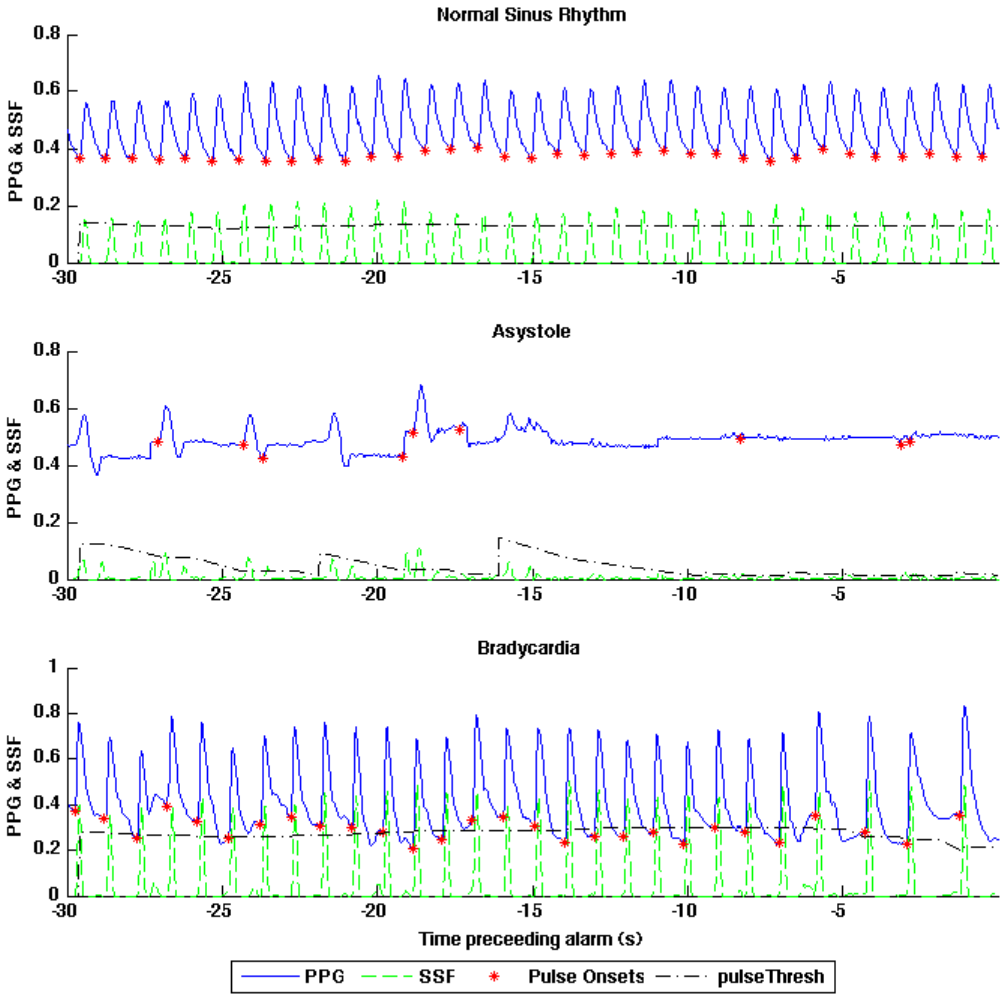

Figure 3-2: PPG pulse onset detection by $aPPG$ under conditions of normal sinus rhythm, asystole, and bradycardia. Under normal sinus rhythm, the amplitude of the PPG waveform stays constant, the pulse confirmation threshold rests at 70% of the pulse amplitude, and the $aPPG$ algorithm detects all the pulses. In the examples of asystole and bradycardia, the pulse confirmation threshold is decreased in expectation of low-amplitude pulses. After 4 refractory periods (1 s) following the last pulse detection, the pulse confirmation threshold decreases at a rate of $d_c \cdot F_s = 12.5\%$ per second until the next pulse is detected and the confirmation threshold is adjusted to the recent amplitude of the waveform. A noise floor is set at 0.0125 to avoid false pulse detections.

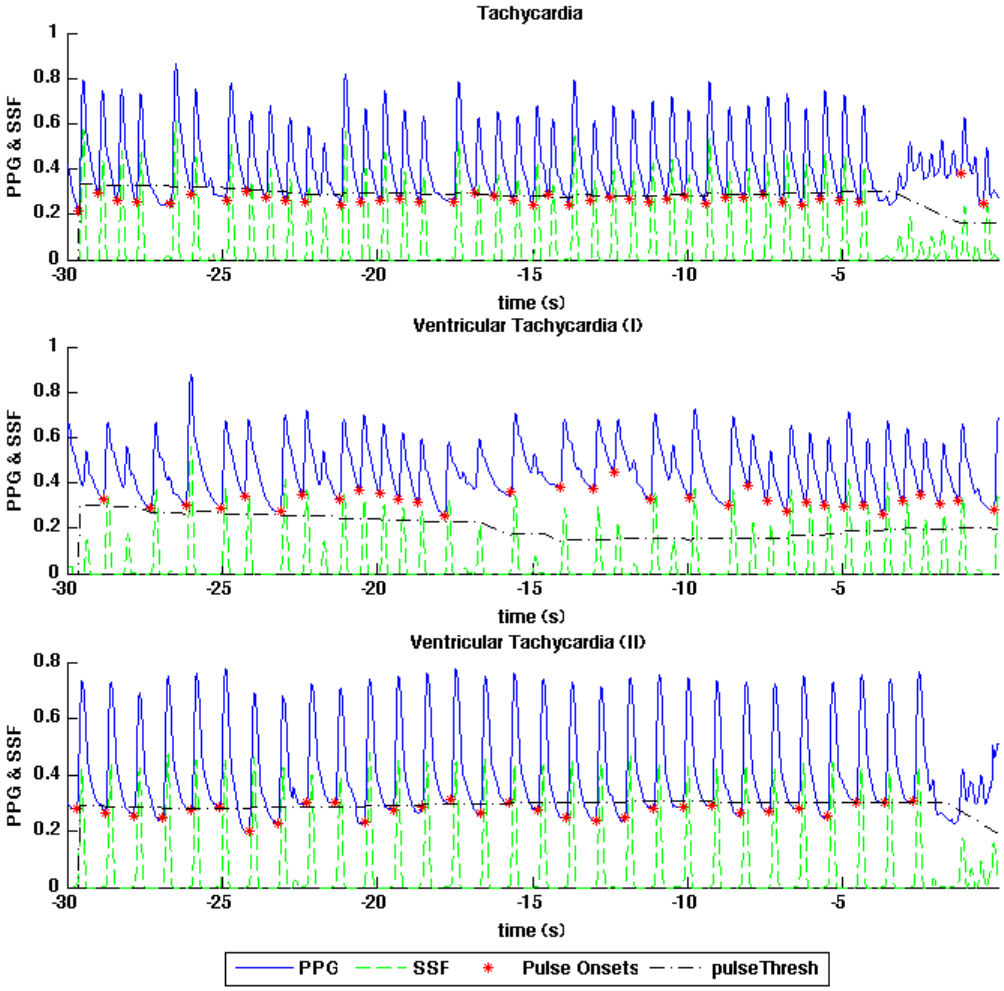

Figure 3-3: PPG pulse onset detection by $aPPG$ under conditions of tachycardia and ventricular tachycardia. At the onset of sustained extreme tachycardia or ventricular tachycardia (illustrated in the top and bottom traces, respectively), a sudden decrease in pulse amplitude is observed. In the case of unsustained ventricular tachycardia (illustrated in the center trace), intermittent rapid beats yield low-amplitude pulses in the PPG. All three cases cause missed detections by the pulse onset detector. After 4 refractory periods (1 s) following the last pulse detection, the pulse confirmation threshold decreases at a rate of $d_c \cdot F_s = 12.5\%$ per second until the next pulse is detected and the confirmation threshold is adjusted to the recent amplitude of the waveform.

excluded from this study. The remaining segments were presumed to contain clean, good quality PPG data, and the corresponding pulse onsets were included in the study.

Annotations for QRS detections in the ECG and pulse onsets in the ABP waveforms are both available for records in the MIMIC I database. A standard open-source beat comparison algorithm, *bxb* [10], with an 800 ms match window to account for pulse transit time was applied to these annotations to find beats appearing in either the ECG or ABP waveforms. With matching beats counted only once, $6,058,072$ beats were found in the two waveform types. ECG and ABP beats appearing while the PPG waveform exhibited signal dropout, flat-line or other gross artifact (such as maximum or minimum saturations or high-frequency noise) were excluded from the analysis. The remaining $4,227,904$ beats (detected from $1,033.4$ hours of waveform data) were used as a surrogate for a gold-standard reference set for evaluating the performance of $aPPG$.

The $aPPG$ algorithm was applied to the PPG waveforms, and detected $3,859,567$ beats in the good-quality waveform segments. These beats were compared to the surrogate reference set using *bxb* with an 800 ms match window.

3.3.2 Results

Of the beats detected in the ECG and ABP waveforms, 87.53% were also detected in the PPG waveform by the algorithm. Of the beats detected by $aPPG$, 95.88% were also annotated pulses in the ECG or ABP waveforms. The sensitivity and positive predictive value of the $aPPG$ algorithm performance over all 31 patients are summarized in Table 3.1.

3.3.3 Discussion of Limitations

Of the pulses detected by the $aPPG$ algorithm, 4.12% did not appear in the ABP or ECG waveforms. However, 12.47% of the pulses which travel from the heart to the periphery are not detected in the PPG. One explanation is that these pulses do

Table 3.1: Performance of *aPPG* on MIMIC I database. TP = true positive (PPG detection also appeared in ECG or ABP); ; FP = false positive (PPG detection did not appear in ECG or ABP); FN = false negative (Pulse detection in ECG or ABP did not appear in PPG.

Record Number	Length of Record (h)	TP	FP	FN	Sensitivity (%)	PPV (%)
466	68.7	249654	6678	26610	90.37	97.39
427	58.5	98134	2234	13323	88.05	97.77
444	54.0	290548	1023	6456	97.83	99.65
430	52.0	190945	815	15805	92.36	99.57
213	51.7	76198	463	7756	90.76	99.40
408	48.3	235952	2738	6931	97.15	98.85
224	46.9	237039	1288	4579	98.10	99.46
439	46.4	235428	2507	9350	96.18	98.95
411	45.6	115489	1238	19111	85.80	98.94
409	43.3	242864	3716	33991	87.72	98.49
454	42.8	120114	7137	41001	74.55	94.39
231	42.7	8537	30427	2836	75.06	21.91
449	42.5	157280	1207	10933	93.50	99.24
254	42.5	146822	1225	15282	90.57	99.17
484	42.0	183598	5444	28372	86.62	97.12
474	38.5	140112	18088	11089	92.67	88.57
442	35.1	97630	1864	46042	67.95	98.13
452	33.7	156110	4397	16679	90.35	97.26
451	31.2	75754	425	27078	73.67	99.44
477	30.0	76136	2911	48336	61.17	96.32
446	27.9	30607	35613	17739	63.31	46.22
216	27.2	106099	20146	13541	88.68	84.04
218	26.0	69079	1371	18099	79.24	98.05
414	25.1	48516	2029	30420	61.46	95.99
410	23.5	92253	1750	7868	92.14	98.14
211	21.6	51243	640	10191	83.41	98.77
230	19.0	47660	331	2370	95.26	99.31
041	14.3	59673	220	1721	97.20	99.63
417	12.2	17033	432	21189	44.56	97.53
472	8.7	40762	673	11561	77.90	98.38
220	1.2	3262	6	1114	74.54	99.82
Sum	1,033.4	3,700,531	159,036	527,373		
Gross					87.53	95.88
Average					83.49	93.42

not reach the periphery with significant volume to be detected. The topology of the cardiovascular system is such that if the heart beats with low cardiac output, pulse volume and velocity is not sufficient to appear at the end of the arterial tree where the PPG is measured. This cannot be concluded definitively by the analysis presented here because the two reference beat sources are recorded using independent sources and are subject to their own artifacts, and the signal quality metric assessment system is not optimal. However, an estimate of ABP pulse pressure prior to each pulse detection could be used to indicate if there is sufficient pulse volume.

The performance analysis could be made more accurate by improving the reference database against which we compare the detected PPG pulse onsets. A large database of expert annotated PPG pulse onsets over a wide range of physiological conditions would be ideal, but creation of such a database is time consuming. A better surrogate for a gold standard reference would be to choose beats appearing in both the ECG and ABP waveforms, rather than the union of the two pulse detection sets used in this study. The reference beat set could be further improved by ensuring the signal quality of the ECG or ABP waveforms by using algorithms such as $wSQI$ [33].

The PPG pulse onset detection algorithm performs moderately "well" compared to $wABP$ under conditions of normal and slow steady heart rates, as illustrated in Figure 3-2. The common incidence of false pulse onset detections during periods of Asystole can be avoided by turning off the pulse detecting feature if the range of the PPG signal is not above a certain threshold, thereby ignoring both truly flat and nearly flat PPG waveform segments.

In the current implementation, the adaptive threshold mechanism does not adapt quickly enough to detect low-volume pulses which result from premature ventricular contractions. Similarly, the algorithm takes too much time to adapt to low pulse volume during sustained tachycardia or ventricular tachycardia. These limitations are illustrated in Figure 3-3. If tachycardia is not sustained, the pulses are likely to remain undetected. One improvement could be to use the electrocardiogram's QRS detections to adapt the pulse threshold. The algorithm also does not adapt quickly enough to a common PPG artifact in which signal saturation to minimum

or maximum for less than one second triggers the monitor to reduce the gain of the waveform by half or more for the next three to five beats.

The performance of $aPPG$ therefore is promising for heart rate estimation. However the limitations posed by sudden gain changes and pulse volume variability could be improved by further tuning or reference to the ECG. Next, we propose a method for tuning the algorithm.

3.3.4 Future Work: Parameter Optimization and Testing

The PPG waveform pulse onset detector has two thresholds, the pulse initiation threshold and pulse confirmation thresholds, which are adapted at separate rates in order to obtain robust performance in the presence of arrhythmias. The pulse confirmation threshold is updated by T_c, the fraction of the difference between the local maximum and minimum values of the SSF. The pulse confirmation threshold is continuously decreased by a fraction, $d_c = 0.1\%$, of the PPG waveform amplitude over the previous 5 s if no new pulse has been detected for more than four refractory periods. To determine the best adaptivity rate settings, T_c and d_c, we should evaluate the performance of the algorithm under various threshold combinations. The PPG pulse morphology varies little when the heart rate and rhythm are constant but deviates during periods of arrhythmia as the stroke volume changes. The $aPPG$ algorithm performs differently at different extremes of heart rate, so we should study the threshold combinations during periods of steady heart rate, variable heart rate,and a combination of steady and varying heart rate (to simulate real-life conditions).

To avoid over-training our data, data from patients with simultaneously recorded ABP and PPG should be split into training and testing sets. A limited number of epochs should be extracted from each patient record to ensure diversity of the training and testing set. The epochs should be selected based on three criteria: (1) that simultaneously recorded PPG and ABP waveforms are available, (2) that at least 90% of the blood pressure waveforms are marked as high signal quality by $wSQI$ [33], and (3) that the PPG segments contain no gross artifacts, signal dropout, or missing data, as determined by the $pSQI$ algorithm presented in Chapter 2.

The PPG segments should be sorted into two groups, one containing data at normal sinus rhythm, and one containing data recorded while the patient has a cardiac arrhythmia. Any PPG segment with a regular heart rate and clear pulses should be sorted into the first category. Any segment with ectopic beats or high variation in heart rate should be sorted into the second category.

The $aPPG$ algorithm should be run over waveforms in both the steady heart rate and arrhythmia categories with varying combinations of T_c and d_c, and the pulse onsets should be recorded. To create a reference set of annotations, $wSQI$ [33] should be run over the simultaneously recorded blood pressure waveform segments. As before, a beat-by-beat comparison should be made between the recorded PPG pulse onsets and the recorded blood pressure pulse onsets. Performance of $aPPG$ should be evaluated under each combination of parameters, and the T_c and d_c values which yield the best performance in each category should be applied to the algorithm and run on the test sets. The performance observed will be the best possible scenario of pulse onset detection, since the waveforms should not contain major artifacts.

Ideally, the steady and variable heart rate data should be mixed in a realistic manner, and the $aPPG$ algorithm should be tested on this third data set. Note that this procedure requires an accurate assessment of the proportion of time which ICU patients have steady versus variable heart rates.

An alternative evaluation procedure might take a stress-test approach, to study the ability of $aPPG$ to reliably detect pulses under varying levels of artifact. In this procedure, one might take clean PPG and ABP data at various steady heart rates, and inject controlled amounts of artifact to the waveforms. The artificial PPG artifacts could be generated in a manner similar to the artificial blood pressure artifacts developed by Li *et al.* [16].

3.4 Use of $aPPG$

Once pulse onset times are established, the waveform can be broken down into individual pulses and the morphology of each pulse can be considered. In this study, we

use pulse onset detections to estimate heart rates in PPG segments recorded while an alarm is triggered in the electrocardiogram monitor.

THIS PAGE INTENTIONALLY LEFT BLANK

Chapter 4

A New False ECG Alarm Suppression Framework Using the PPG Waveform

Using the *aPPG* pulse onset detector and *pSQI* signal quality algorithms, we form a new framework to suppress false critical ECG alarms by estimating heart rate and studying pulse morphology in the PPG waveform.

4.1 Algorithm Architecture

In Section 1.1 and Appendix A, we reviewed the work of Aboukhalil *et al.*, who created a false ECG alarm suppression framework which utilises the arterial blood pressure waveform to estimate heart rate and suppress heart-rate related alarms. This algorithm first checks the signal quality of all detected beats in the ABP segment, accepting the alarm if the signal quality is poor. Then the algorithm employs a system of logic which considers the quality and morphology of each detected pulse, and the instantaneous heart rate estimated from those pulses, to determine if the ECG alarm should be accepted or suppressed. The details of the logic employed by this framework are included in Appendix A, as well as the performance of the algorithm on the alarm data described in Section 2.3.2.

We take a similar approach to assessing the validity of critical ECG arrhythmia alarms using the PPG waveform. We utilise the windowing parameters which were found to yield optimal alarm suppression performance in the study by Aboukhalil *et al.* At the onset of each alarm, we extract a 17-second segment of PPG data, extending from 13 seconds before the alarm to 4 seconds after the alarm. Next, we apply the $pSQI$ signal quality metric. In our framework we consider each type of alarm separately, applying Hjorth parameter thresholds to determine signal quality depending on the alarm type. If at least 80% of the windowed PPG signal is marked as high quality according to the applied thresholds, then the heart rate is estimated from the beat onsets detected by the $aPPG$ algorithm. The ECG alarm is then flagged as true or false depending on whether the heart rate is within the error tolerances found to be optimal by Aboukhalil *et al* [1].

Because our PPG signal quality metric does not function on a beat-by-beat basis, we do not study the number of beats with abnormal pulse morphologies. However, we can use certain aspects of PPG phenomenology to support the logic based on heart rate estimation. Specifically, we use the observation that during episodes of extreme tachycardia and ventricular tachycardia, the pulse volume may decrease due to low stroke volume. The sudden decrease in pulse amplitude causes several missed pulse detections when the $aPPG$ algorithm is used to mark the onset of each PPG pulse (see Section 3.3.3), yielding long intervals between detected beats. Therefore, in place of pulse morphology analysis, we construct a framework based on PPG-based heart rate estimation and pulse duration.

At the onset of each critical ECG arrhythmia alarm, a 17-second PPG waveform segment is extracted from 13 seconds prior the alarm to 4 seconds after. Alarms where the PPG waveform is not available for this 17-second window were excluded from the study. Next, the $pSQI$ algorithm is used to assess the signal quality of the extracted PPG segment. If less than 80% of the duration of the PPG waveform is marked as high signal quality, the PPG signal quality of the 17-second segment is judged to be poor and the ECG alarm is accepted as true. Otherwise, the $aPPG$ algorithm is applied to detect PPG pulse onsets. To reduce false pulse detections

by the $aPPG$ algorithm, the noise floor on the slope sum function is increased from $T_n = 0.0125$ to $T_n = 0.02$. The new value of T_n was chosen to eliminate true asystole alarm suppressions in the training set without decreasing false alarm suppression. Finally, the following logic is employed to assess the validity of the alarm depending on the alarm type. Figure 4-1 illustrates the algorithm architecture where the PPG signal quality is sufficiently high. The windowing and thresholding parameters used in the PPG-based false alarm suppression algorithm are summarized in Table 4.1.

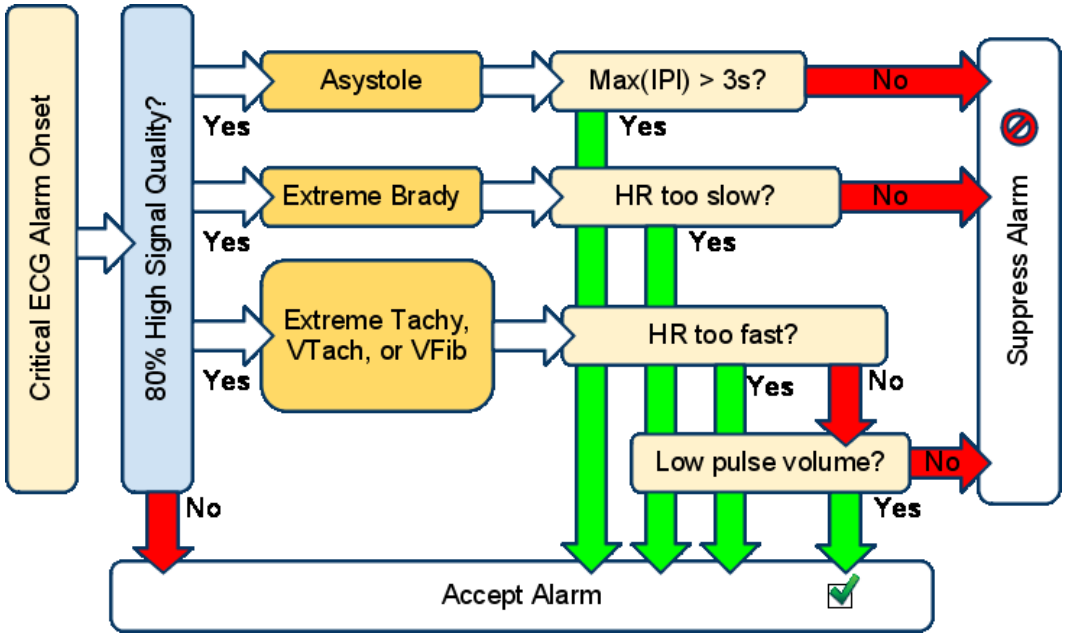

Figure 4-1: False ECG Alarm Suppression Using the PPG Waveform. If at least 80% of the 17-second PPG segment is high signal quality, this logic is used to determine if the alarm should be accepted or suppressed. IPI = inter-pulse interval.

4.1.1 Asystole Processing

From the detected pulse onsets, the largest pulse-to-pulse interval (for the case where the asystole resolves itself within the window) and the interval between the last detected pulse and the end of the window (for the case where asystole lasted beyond the analysis period) are calculated. If either of these intervals exceeds $T_A = 3$ s, the absence of beats is noted and the asystole alarm is accepted; otherwise it is suppressed.

4.1.2 Extreme Bradycardia Processing

Bradycardia alarms in the ECG waveforms are marked relative to a heart rate threshold set on the monitor. The $N_B = 3$ longest pulse-to-pulse intervals are calculated. If the mean heart rate calculated from these intervals is within $E_B = 7$ beats per minute of the monitor's heart rate, then the bradycardia alarm is accepted; otherwise it is suppressed.

4.1.3 Extreme Tachycardia Processing

Tachycardia alarms in the ECG waveforms are marked relative to a heart rate threshold set on the monitor. The ($N_T = 1$) shortest pulse-to-pulse interval is calculated. If the heart rate calculated from this interval is less than $E_T = 20$ beats per minute over the threshold set on the monitor, and the longest pulse-to-pulse interval is less than $T_{NoPulse} = 1.8$ s long (indicating no missed detections due to loss in pulse volume), then the tachycardia alarm is suppressed.

4.1.4 Ventricular Tachycardia Processing

A ventricular tachycardia alarm is accepted if either the longest pulse-to-pulse interval is greater than $T_{NoPulse} = 1.8$ s (indicating missed detections due to loss in pulse volume) or the heart rate calculated from the ($N_{VT} = 1$) shortest pulse-to-pulse interval exceeds $R_{VT} = 80$ beats per minute. Otherwise, the alarm is suppressed.

4.1.5 Ventricular Fibrillation Processing

Ventricular fibrillation alarms are suppressed if the longest pulse-to-pulse interval is less than $T_{NoPulse} = 1.8$ s (indicating no missed detections due to loss in pulse volume) and the heart rate calculated from the ($N_{VF} = 1$) shortest pulse-to-pulse interval is less than $R_{VF} = 150$ beats per minute. Otherwise, the alarm is accepted.

Table 4.1: Windowing and thresholding parameters in merged PPG-based false alarm suppression algorithm. "PPI" signifies pulse-to-pulse interval. "N/A" signifies that the parameter is not applicable.

Parameter ⇒ Alarm Type ⇓	Max. PPI length (s)	HR error margin (bpm)	Intervals for HR calc.	HR Threshold (bpm)
Asystole	$T_A = 3$	N/A	N/A	N/A
Extreme Bradycardia	N/A	$E_B = 7$	$N_B = 3$	N/A
Extreme Tachycardia	$T_{NoPulse} = 1.8$	$E_T = 20$	$N_T = 1$	N/A
Ventricular Tachycardia	$T_{NoPulse} = 1.8$	N/A	$N_{VT} = 1$	$R_{VT} = 80$
Ventricular Fibrillation	$T_{NoPulse} = 1.8$	N/A	$N_{VF} = 1$	$R_{VF} = 150$

4.2 Optimization of Signal Quality Thresholds

To determine the optimal settings to use in the $pSQI$ algorithm for each arrhythmia type, the number of true and false alarms in the training set suppressed by this PPG-based framework were recorded using 512 combinations of Hjorth parameter thresholds, η_1^l,η_1^l, and η_2, chosen from the distributions computed in Section 2.3.5 (see Figures 2-4 and 2-5). Table 2.6 lists the thresholds settings which were examined. The false and true alarm suppression rates are illustrated in Figures 4-2 through 4-5.

We chose parameter thresholds which maximized false alarm suppression while minimizing true alarm suppression. This is possible for asystole, bradycardia, and extreme tachycardia alarms, even if the set of thresholds where these two critera are met is small (as is the case for extreme bradycardia and extreme tachycardia alarms). However, for ventricular tachycardia alarms there was no combination of ${\eta_1}^l$, ${\eta_1}^u$, and η_2 which maximized false alarm suppression while minimizing true alarm suppression. This meant we could not suppress any number of false alarms without also suppressing some true alarms in this category. For asystole, bradycardia, and extreme tachycardia alarms, we choose to set the Hjorth parameter thresholds in the centroid of the volume defined by those which yielded the highest false alarm suppression rate and the lowest true alarm suppression rate. These volumes are marked using solid pink dots and

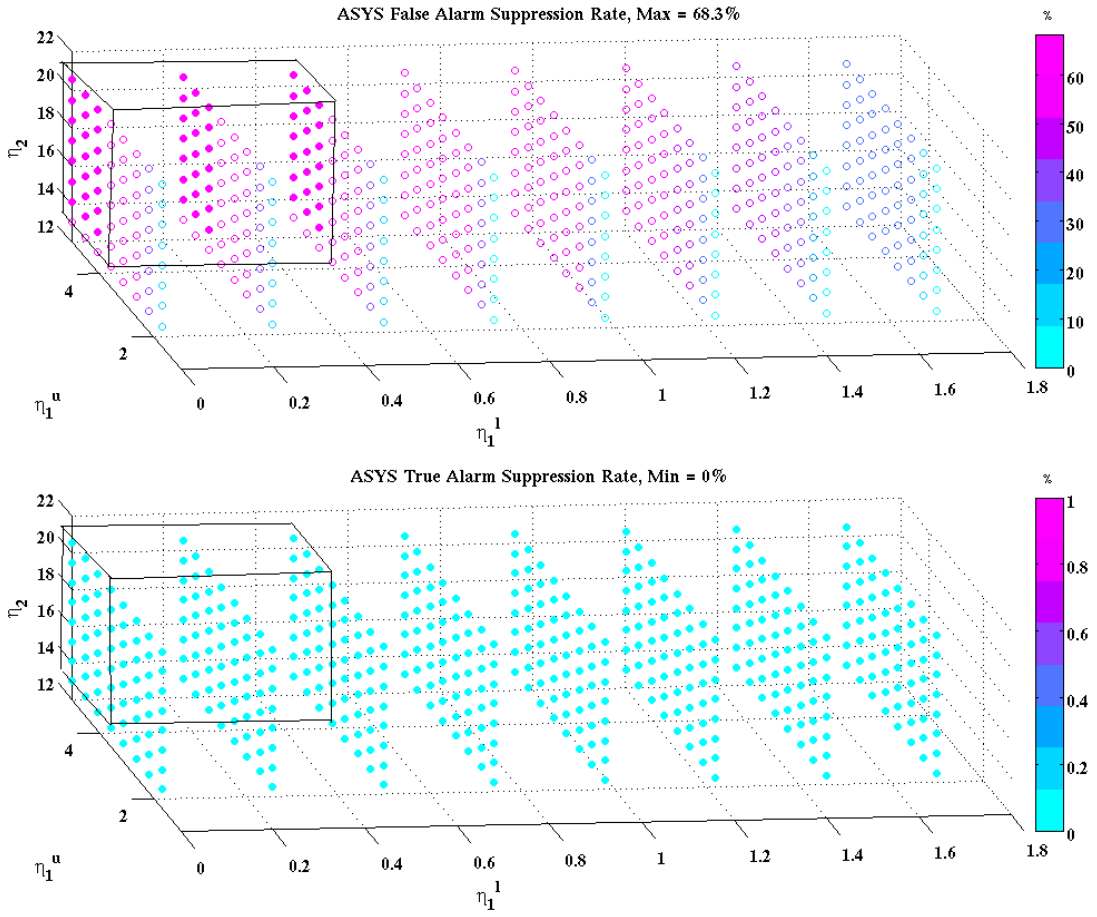

Figure 4-2: Effect of η_1^l,η_1^u, and η_2 on true and false alarm suppression rates during asystole. In the top plot, solid pink dots mark the highest false alarm suppression rate. In the bottom plot, solid blue dots mark the lowest false alarm suppression rate. The set of thresholds which maximize false alarm suppression while minimizing true alarm suppression are outlined.

solid blue dots, respectively, in Figures 4-2 through 4-5. For ventricular tachycardia alarms, we choose to set the Hjorth parameter thresholds in the centroid of the volume defined by those which yielded the highest false alarm suppression rate. The selected threshold settings are summarized in Table 4.2.

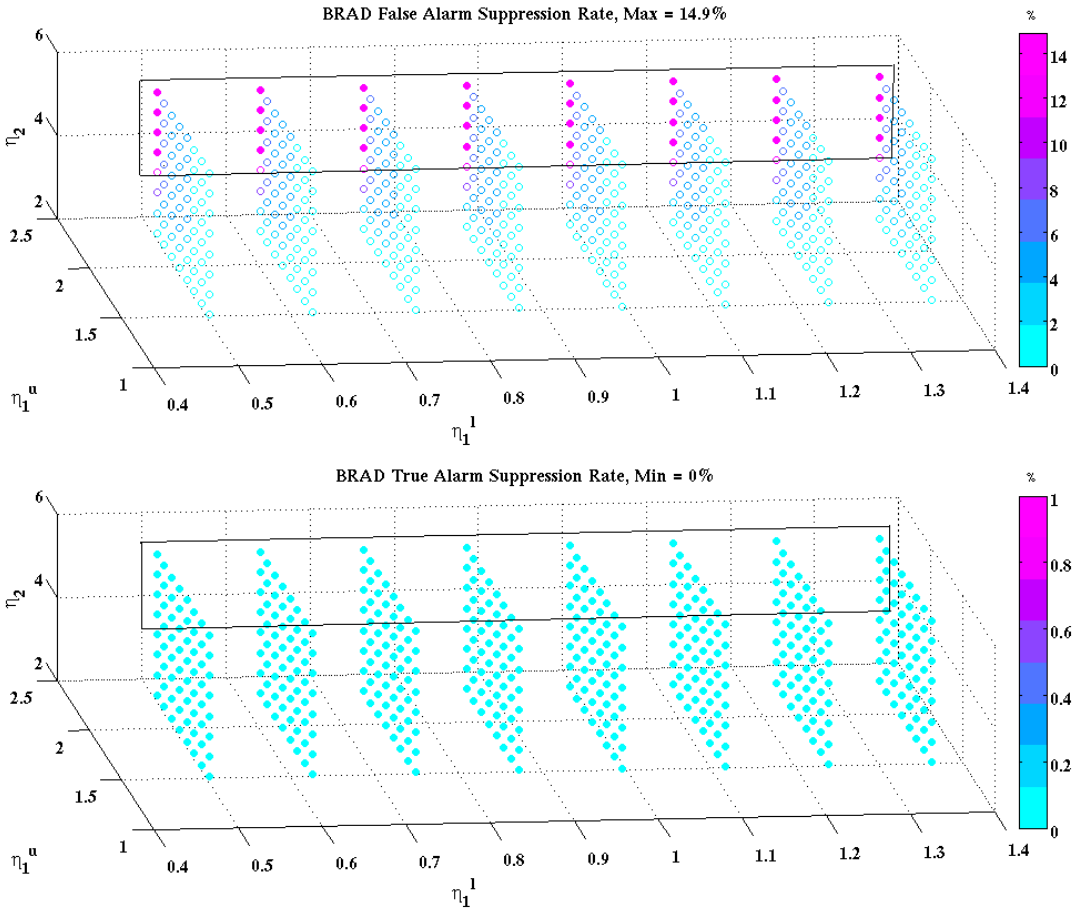

Figure 4-3: Effect of η_1^l,η_1^u, and η_2 on true and false alarm suppression rates during extreme bradycardia. In the top plot, solid pink dots mark the highest false alarm suppression rate. In the bottom plot, solid blue dots mark the lowest false alarm suppression rate. The set of thresholds which maximize false alarm suppression while minimizing true alarm suppression are outlined.

Table 4.2: Optimal assignment of Hjorth parameter thresholds by alarm type using training data

Alarm Type	Threshold Setting		
	η_1^l	η_1^u	η_2
Asystole	0.24	4.49	17.38
Extreme Bradycardia	0.92	2.17	5.06
Extreme Tachycardia	1.66	2.68	7.15
Ventricular Tachycardia	0.82	2.45	3.98

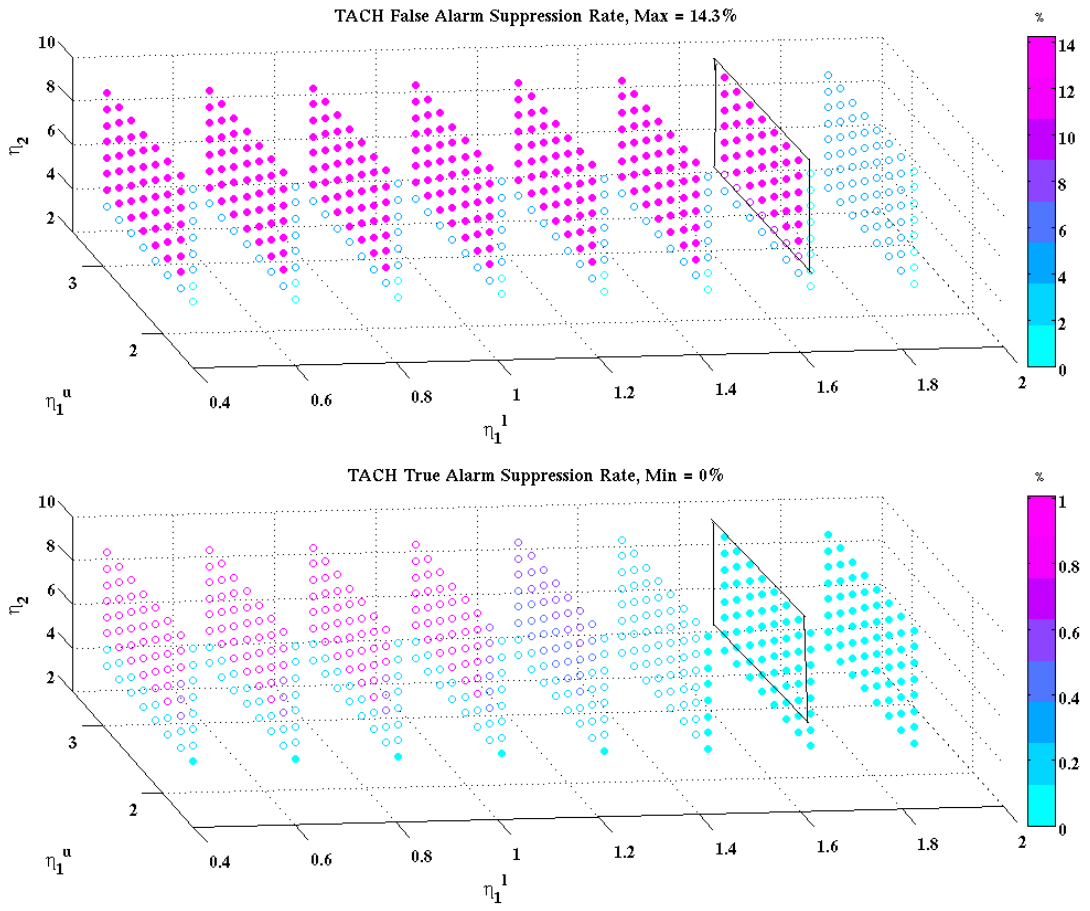

Figure 4-4: Effect of η_1^l,η_1^u, and η_2 on true and false alarm suppression rates during extreme tachycardia. In the top plot, solid pink dots mark the highest false alarm suppression rate. In the bottom plot, solid blue dots mark the lowest false alarm suppression rate. The set of thresholds which maximize false alarm suppression while minimizing true alarm suppression are outlined.

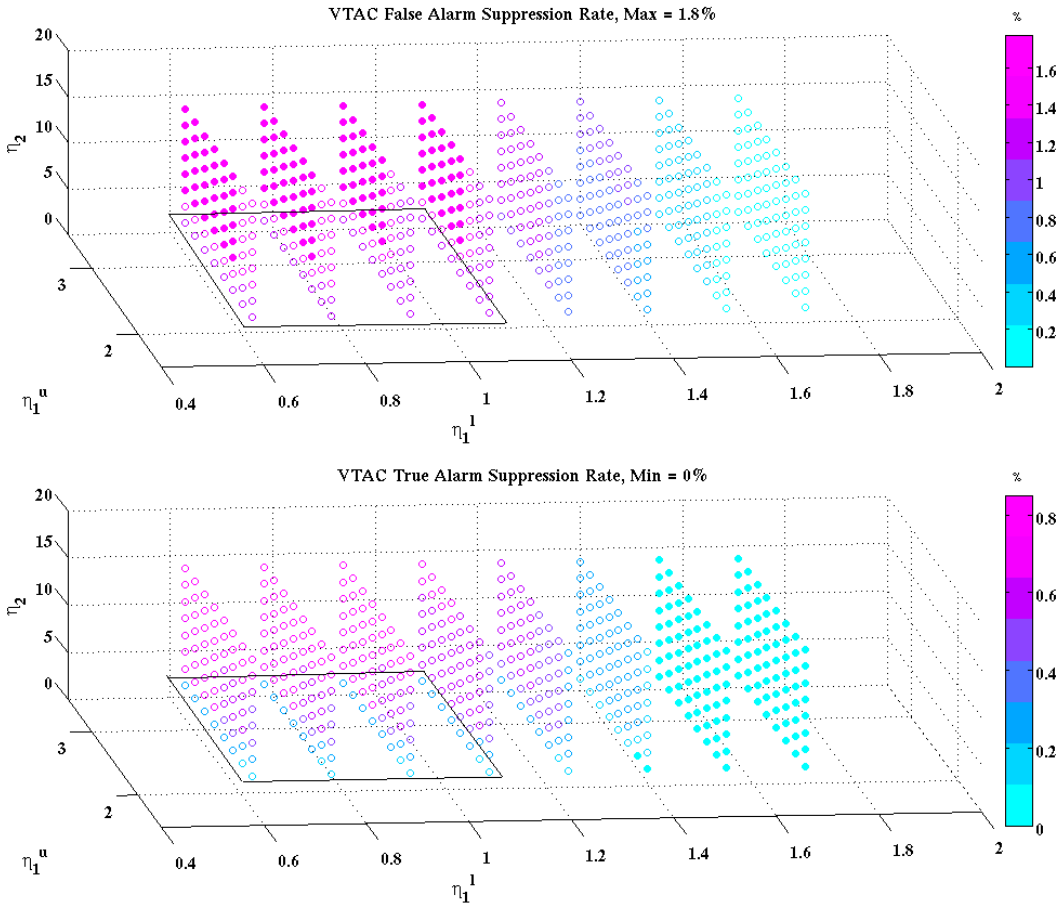

Figure 4-5: Effect of η_1^l,η_1^u, and η_2 on true and false alarm suppression rates during ventricular tachycardia. In the top plot, solid pink dots mark the highest false alarm suppression rate. In the bottom plot, solid blue dots mark the lowest false alarm suppression rate. The set of thresholds which maximize false alarm suppression while minimizing true alarm suppression are outlined.

Table 4.3: Performance of PPG-based false alarm suppression algorithm on new MIMIC II data. Note that ventricular fibrillation/tachycardia alarms are combined with and annotated as ventricular tachycardia alarms. "FA" signifies false alarm. "TA" signifies true alarm. "FA Rate Before" and "FA Rate After" refer to the false alarm rate before and after the modified suppression algorithm was used, respectively.

Alarm Type	Data Set	TA Suppression	FA Suppression	FA Rate Before	FA Rate After
Asystole	Training	0%	68.3%	91.7%	29.0%
	Testing	9.5%	68.0%	92.8%	29.7%
	Combined	**4.0%**	**68.2%**	**92.2%**	**29.3%**
Ext. Brad.	Training	0%	14.9%	36.1%	30.7%
	Testing	0%	35.7%	18.0%	11.5%
	Combined	**0%**	**20.6%**	**28.3%**	**22.4%**
Ext. Tach.	Training	0%	14.3%	4.1%	3.5%
	Testing	2.3%	2.0%	15.7%	15.3%
	Combined	**0.8%**	**5.7%**	**8.4%**	**8.0%**
Vent. Tach.	Training	0.3%	1.4%	41.8%	41.2%
	Testing	0%	1.7%	55.2%	54.2%
	Combined	**0.2%**	**1.6%**	**48.0%**	**47.2%**
All	Training	0.2%	26.0%	40.3%	29.9%
	Testing	0.9%	22.1%	51.1%	39.8%
	Combined	**0.5%**	**24.0%**	**45.1%**	**34.3%**

4.3 Performance of PPG-Based False Alarm Suppression

The performance of the PPG-based false alarm suppression algorithm applied to the training and test sets is summarized in Table 4.3. Across the entire collection of alarms in both the training and test sets, the PPG-based algorithm suppressed 0.5% of the true alarms and 24.0% of the false alarms.

On the training set, the algorithm suppressed true alarms only in the ventricular tachycardia category. However in the test set, the PPG-based system suppressed true alarms in two categories: asystole and extreme tachycarida. The highest rate of true alarm suppression was in the asystole category. In the test set, 9.5% (or 2 of 21) of true asystole alarms were suppressed. In both of these cases the PPG waveform exhibited mid-frequency wave-like artifacts (most likely due to motion) but were not marked as poor signal quality using the $pSQI$ algorithm and asystole thresholds chosen in Table

4.2. The $aPPG$ algorithm falsely detected pulses in these segments. This behavior may be addressed by raising the noise floor in the $aPPG$ algorithm.

The false alarm suppression performance of the PPG-based system varies widely from one alarm category to another. Across both training and test sets, the algorithm suppressed 68.2% of false asystole alarms, but only 1.7% of false ventricular tachycardia alarms. The algorithm also suppressed only 1.6% of false extreme tachycardia alarms in the test set. The low false alarm suppression rate in this category is often due to poor signal qualtiy or heart rate estimates which exceeded the threshold of the false alarm suppression algorithm. Raising the ventricular tachycardia rate threshold, R_{VT}, to 100 bpm raised the combined false alarm suppression rate to 5.7% but also increased the true alarm suppression rate to 3.1%.

4.4 Limitations and Possible Improvements

The method of splitting our data into training and test sets was designed to keep the number of patients equal for each alarm type. The poorer performance on the test set indicates an asymmetry in the quality of signals and number of alarms investigated in the training and test sets, with some circumstances arising in the test set which did not appear in the training data. While the relative frequency of alarm types in this study were similar in the training and test sets (see Tables 2.2 through 2.4), the total alarm counts were unequal, illustrating that patient records do not contribute equally to each alarm category and greatly in the number of alarms triggered. If similar studies are to be performed in the future, we recommend that five fold cross-validation is used to compensate for this imbalance.

Using the methods of PPG signal quality assessment and pulse onset detection described in Chapters 2 and 3 of this thesis, the false ECG alarm suppression framework using the PPG waveform does not perform as well as a similar framework which utilizes the ABP waveform. The algorithm suppressed fewer false alarms than the ABP-based system of Aboukhalil *et al* in all alarm categories and only had a large impact for asystole alarms. Moreover, non-zero true alarm suppression rates are

probably clincally unacceptable for the asystole category. Fewer than 30% of false alarms were suppressed in the case of extreme bradycardia, though no true alarms were suppressed. The extreme tachycardia and ventricular tachycardia categories had false alarm suppression rates as low as 5.7% and 1.6%, respectively, making the algorithm of marginal use for these alarm types. Therefore it is hard to recommend the approach described here for any alarm cateogories other than asystole and extreme bradycardia. Even in the case of asystole, parameters may need further refinement to reduce the true alarm suppression rate from 4% down to almost 0%.

The correlation between noise in the ECG channels and noise in the PPG waveform has not been investigated. Artifacts in both channels may be due to the same source, such as patient movement. This is a fundamental limitation to the PPG-based false alarm suppression approach, especially because the PPG signal is highly sensitive to movement. Correlations between ECG noise and PPG noise, as well as corellations between detected ECG and PPG beats should be examined.

The false alarm suppression algorithm could not be evaluated in the case of ventricular fibrillation because there were no instances of true ventricular fibrillation alarms in the training or test data, and the ventricular fibrillation/tachycardia and ventricular tachycardia alarms were combined into one category.

The components of the PPG-based false alarm suppression framework could be improved and tuned in several ways. The windowing parameters and heart rate thresholds used by the ABP-based false alarm suppression system of Aboukhalil *et al.* [1] should be varied to find the optimal settings for this data set. In particular, the heart rate thresholds for tachycardia and ventricular tachycardia should be investigated.

Extreme bradycardia and extreme tachycardia alarms are issued with the heart rate threshold used by the monitor. The false alarm suppression rates for extreme bradycardia and extreme tachycardia could be improved by using this heart rate threshold as an input parameter to the $aPPG$ algorithm. This would adjust the refractory period of the pulse onset detector, and may improve heart rate esitmation in these two alarm categories. However the method assumes the alarm is true, and

may not work if the heart rate greatly differs from the threshold on the monitor.

Like the ABP-based algorithm, the PPG-based false alarm suppression framework has particular difficulty with examining periods of unsustained ventricular tachycardia. This arrhythmia occurs if there is a ventricular rhythm (that is, one consisting of beats which originate in the ventricles rather than from the sinoatrial node) with a rate over 100 beats per minute, and is diagnosed using the electrocardiogram waveform. At low heart rates, the ABP and PPG waveforms cannot be used to infer these details of the morphology of the ECG QRS complexes, and can only show the presence of a beat. If the rate of the tachycardia is low enough (for example, $100 - 130$ bpm), the morphologies of the ABP or PPG pulses corresponding to these ventricular beats appear to be normal. If in the future a similar logical structure is to be used for false ventricular tachycardia alarm suppression, we recommend that the R_{VT} heart rate threshold be adjusted to increase the number of false alarms suppressed. However, this may result in a larger number of true alarm suppressions.

THIS PAGE INTENTIONALLY LEFT BLANK

Chapter 5

Conclusions

5.1 Summary

5.1.1 Contributions

In this thesis we examined an algorithm which analyzes the PPG waveform for information to use in the suppression of false critical ECG arrhythmia alarms issued by ICU bedside monitors. To meet this goal, a signal quality metric, $pSQI$, and a pulse onset detection algorithm, $aPPG$, were created to evaluate the fidelity of the PPG signal and to assist in heart rate estimation.

A database of $4,326$ annotated critical life-threatening ECG alarms was created to tune the $pSQI$ algorithm thresholds and evaluate the PPG-based false alarm suppression system. For benchmarking the performance of this new false alarm suppression framework, the ABP-based algorithm of Aboukhalil *et al.* [1] was corrected to check for low-volume pulses in the presence of extreme tachycardia, ventricular tachycardia, or ventricular fibrillation alarms.

5.1.2 Evaluation and Limitations

Annotations of the alarms were made by individuals who were not involved in the creation of the ECG arrhythmia detection algorithms used in the ICU bedside monitors. ECG alarms were therefore annotated using clinical criteria, and our alarm definitions

may not be completely consistent with the logic used by the monitoring algorithms in some cases. The annotations for the "ventricular fibrillation/tachycardia" alarm category in particular may not be consistent. The monitor algorithm fired an alarm upon the detection of rapid ventricular tachycardia. The clinical annotator lableled rapid ventricular tachycardia as "ventricular tachycardia" and the ventricular fibrillation annotation was reserved for asynchronous ventricular electrical activity. The database did not show any true ventricular fibrillation events.

This annotation methodology affects the performance of the PPG signal quality algorithm, $pSQI$. We quantified the spectral characteristics of the PPG waveform using Hjorth parameters. PPG waveform segments corresponding to true alarms in each category exhibit different heart rates and morphologies, and therefore have different spectral characteristics. The Hjorth parameter thresholds for determining the quality of the PPG signal are therefore set depending on the alarm type. The Hjorth parameter thresholds chosen for ventricular tachycardia alarms in this study will not provide the best assessment of signal quality under the condition of true ventricular fibrillation.

The $aPPG$ algorithm is limited in its ability to detect low-volume pulses. Recall that the algorithm has an adaptive pulse confirmation threshold, which updates to $T_c\%$ of the recent pulse amplitude when a pulse is detected, and decreases at a rate of $d_c\%$ per sample point (or $F_s \cdot d_c\%$ per second, where F_s is the sampling frequency) when a pulse is not detected within 4 refractory periods. To avoid false pulse detections due to low-amplitude artifacts, a noise floor is set at half of the smallest expected true pulse amplitude. If the threshold is decreased below the noise floor, it is reset to a value based on the recent amplitude of the PPG waveform. The rate at which the pulse confirmation threshold adapts (d_c) after a pulse has not been detected for some time, and the value relative to the recent waveform amplitude (T_c) to which that threshold adapts when a pulse is detected, have not been rigorously evaluated during different arrhythmias. A trade-off in the noise floor setting exists when we wish to detect pulses at different heart rates. In particular, if we wish to detect low-amplitude pulses in the PPG waveform which appear during periods of extreme

tachycardia or ventricular tachycardia, the noise floor should be set at a low value to increase sensitivity of the pulse detection algorithm. However, in the case of asystole alarms we wish to decrease the sensitivity of the algorithm to artifactual oscillations in the waveform to prevent false pulse detections.

The PPG-based false alarm suppression system does not perform as well as the ABP-based suppression system with similar logic when both algorithms were applied to the same set of annotated ECG alarms. The PPG-based algorithm performed best in the asystole category, suppressing 68.2% of false asystole alarms and 4.0% of true asystole alarms over both the training and test sets. False asystole alarms, false extreme tachycardia alarms, and false ventricular tachycardia alarms comprise the bulk of the false alarms in our data set. However, non-zero true alarm suppression exists for the asystole, extreme tachycardia, and ventricular tachycardia categories, as well as low false alarm suppression rates in the extreme tachycardia and ventricular tachycardia categories. This indicates that if the asystole true alarm suppression rate can be reduced 4.0% to 0% this algorithm will be of use in false asystole alarm suppression.

5.2 Future Work

The application of the *aPPG* and *pSQI* algorithms in the false alarm suppression framework highlighted several improvements which could be made to the pulse onset and artifact detectors.

5.2.1 *pSQI* Improvement

The artifact detector uses a short window length in which to assess the quality of the PPG waveform. In this study we have used 2 s non-overlapping windows in order to make the artifact detector sensitive to the sudden onset of a disruptive artifact. Overlapping the windows may decrease the sensitivity of the artifact detector to these sudden artifacts. The effect of the choice of window size on the accuracy of the Hjorth parameter estimates and the ability to detect artifacts should be evaluated.

The generation of artificial PPG artifacts, in a manner similar to Li *et al.* [16] may be useful in conducting a controlled study of PPG artifact detection.

In this study, the Hjorth parameters were estimated from 30 s of PPG data preceding the onset of each ECG arrhythmia alarm. When this method for training the Hjorth parameter thresholds was used, the false alarm suppression algorithm often failed where the ECG exhibited an intermittent, non-sustained arrhythmia. For a more accurate description of the range of Hjorth parameter values under each alarm condition, the Hjorth parameters should be calculated from data where the arrhythmia is present for the entire duration of the segment, such as 10 seconds surrounding the alarm.

The distributions of H_1 and H_2 parameters illustrated in 2-4 and 2-5 are assumed to take most of their "mass" from clean PPG waveforms. However, this assumption was never tested. The alarm annotations were based on the morphology of the ECG waveform. In future work, PPG segments with Hjorth parameters which lie within the interquartile range should be examined to ensure that the PPG waveform morphology is characteristic of the issued alarm.

Several settings of Hjorth parameter thresholds were investigated for each alarm type to determine the proper signal quality thresholds for each arrhythmia. Figures 4-2 through 4-5 illustrate the effect of the Hjorth parameter threshold settings on the performance of the PPG-based false alarm suppression algorithm. In some alarm categories, the set of thresholds which yielded maximum false alarm suppression while minimizing true alarm suppression is very small. The range of the ${\eta_1}^u$ and η_2 thresholds tested should be extended until the false alarm suppression rate levels off, especially in the extreme bradycardia alarm category.

As an alternative to a frequency-based signal quality metric, the use of dynamic time warping of a matched filter or adaptive template could be evaluated, using cross-correlation to quantify the extent to which each detected pulse deviates from normal pulse morphology. Rapid non-physiological oscillations in oxygen saturation could also serve as an estimate of signal quality in the PPG waveform; if oscillations in the corresponding oxygen saturation estimates occur which are too rapid, the underlying

PPG waveform is likely to have been corrupted by artifact. However, the oxygen saturation time series available to us may be too heavily filtered for this purpose. Analysis using the raw waveform data from the pulse oximeter should be conducted if possible, rather than using the signal which has been post-processed by the bedside monitor or pulse oximeter module.

5.2.2 $aPPG$ Improvement

A rigorous evaluation of the parameters of the pulse onset detector should be conducted. For this evaluation, a database of annotated PPG pulse onsets should be created, rather than using beat onsets from other waveforms, as was conducted in this study.

Various settings of the threshold adaptivity rate, d_c, and the threshold saturation rate, T_c, should be performed on clean PPG waveforms exhibiting a range of heart rates. A study of the sensitivity of the pulse onset detector to the noise floor setting should be conducted.

Within the application of the $aPPG$ algorithm to false ECG alarm suppression, we should consider using the heart rate or alarm type reported by the monitor as an input parameter to the $aPPG$ algorithm. The refractory period in the $aPPG$ algorithm can be made longer or shorter based on the monitor's heart rate threshold for extreme bradycardia and extreme tachycardia alarms, which may improve pulse onset detection performance. It may be the case that if the pulse threshold adapts more quickly and the noise floor is lowered under tachycardia conditions, low-amplitude pulses may be detectable. Similarly, if the noise floor is raised under asystole conditions, false PPG pulse detections may prevent a true alarm from being suppressed. However, this method risks decreasing the performance of the $aPPG$ algorithm if the alarm is false and the heart rate estimates from the ECG monitor and PPG waveform are very different.

Future uses of the $aPPG$ algorithm include a statistical analysis of the PPG pulse amplitude and pulse duration, pulse transit time, and comparisons to the morphology of the ECG and ABP activity immediately before any particular PPG pulse. That

is, if all are abnormal in a consistent manner, this may indicate the existence of an arrhythmia.

5.2.3 False Alarm Suppression Improvement

The logic used to suppress false asystole and ventricular fibrillation alarms should be improved. In both of these cases, the PPG waveform should not exhibit pulses, since the heart is not pumping. Therefore, the same logic could be employed to suppress false alarms in these categories.

The power spectrum of a non-pulsatile waveform does not exhibit any dominant frequencies, and is instead characterized by the frequency components of noise. Thresholding the power spectrum of PPG waveform segments which accompany true asystole alarms does not differentiate between noise and a non-pulsatile PPG signal. The alarms should instead be suppressed if a pulsatile waveform is detected. When assessing signal quality, rather than setting wide thresholds on the Hjorth parameters to check for a non-pulsatile waveform, the power spectrum should have a dominant frequency estimate (H_1) which lies between the Hjorth parameter ranges of true bradycardia to true tachycardia. If the power spectrum exhibits characteristics of a pulsatile signal, and pulses are detected in the PPG waveform, then the asystole or ventricular tachycardia alarm should be suppressed.

False alarm suppression could be improved by combining the PPG-based framework with the blood pressure framework where both signals are available. The combination of these two systems could be as simple as taking the output of the ABP-based false alarm suppression system where it is available. Alternatively, the outputs could be combined depending on the alarm type. For example, if either the ABP or PPG waveforms contain detectable pulses in the presence of an asystole alarm, the alarm may be marked as false.

The PPG signal quality framework could also be integrated into the robust estimation framework described by Li *et al.* and Nemati *et al.* [15, 16, 21]. This framework uses signal quality metrics and Kalman filter-based innovation metrics to quantify the relationships between simultaneously recorded ECG, ABP, respiration,

and PPG waveforms for continuous, robust heart rate, blood pressure, and respiration estimation. Li *et al.* [16] have shown that fusing heart rate estimates from ECG and ABP can improve the false alarm suppression rates for bradycardia and tachycardia. It would be a simple extension to add the heart rate derrived from the PPG waveform into this framework.

5.2.4 Other applications

A combination of PPG signal quality analysis and pulse onset detection could aid in a study on detection of dampening in the ABP waveform. These algorithms could also be applied to a study of the detection of vasoconstriction, by examining the PPG pulse amplitude and the pulse transit time between each ABP pulse onset detection and the corresponding PPG pulse onset detection.

5.3 Extensibility

The false alarm suppression algorithm presented in this thesis applies as an extension of multi-state system tracking methods being researched at the Charles Stark Draper Laboratory. As part of a space technology program, Draper has been working on the Multi-State Excursion Assessment (MSEA) algorithm, a generic system monitoring and state enunciation algorithm. Originally developed for monitoring the "health" of a vehicle trajectory, the MSEA algorithm monitors multiple vehicle parameters and states, such as position, altitude, and velocity to determine if the landing objective is attainable or unattainable. Nominal values and tolerable error margins are provided for each monitored state and regularly updated. Note that the MSEA algorithm does not identify corrections to undesired states.

The MSEA algorithm could also be applied to physiologic monitoring. In this setting, states might include fiducial markers in physiologic waveforms (such as QRS complexes or pulse onsets) and derived parameters may include heart rate or blood oxygen saturation estimates. Such an envelope system for physiologic monitoring may behave similarly to monitoring technology found in implantable medical devices

or bedside monitors found in hospital ICUs.

The MSEA algorithm relies on the assumption that state information received from sensor inputs is valid and not corrupted. In the presence of corrupt inputs, the MSEA algorithm might return a false or invalid assessment of whether the landing objective is attainable. The MSEA algorithm could therefore benefit from an envelope system which assesses the validity of the received state estimates and determines if the MSEA algorithm output is true. The physiologic monitoring MSEA algorithm extension may behave similarly to the PPG signal quality assessment components of the alarm suppression algorithm presented in this thesis. The envelope system for trajectory assessment might instead perform this verification using mutual information between related states, for example to estimate velocity from previously recorded positions.

Appendix A

False ECG Alarm Suppression Using the ABP Waveform

Clifford *et al.* and Aboukhalil *et al.* have created a logical framework to suppress false heart-rate related alarms issued by ECG bedside monitors in ICU settings [3, 1]. The logic and reported performance of this false alarm suppression framework is briefly reviewed in this appendix. For benchmarking of the PPG false alarm suppression framework described in Chapter 4, the ABP framework was also applied to the data set described in Sections 2.3.1 and 2.3.2. The performance on this new data set are also included in this appendix.

A.1 Original Algorithm Architecture

At the onset of each critical ECG arrhythmia alarm, a 17-second ABP waveform segment is extracted from 13 seconds prior the alarm to 4 seconds after. Alarms where the blood pressure waveform was not available for this 17-second window were excluded from the study. Next, the $wABP$ algorithm [32] is applied to determine the onset time of each pulse in the ABP waveform, and the signal quality index of each detected beat is calculated using the negated output of the $jSQI$ algorithm [26]. At the end of this processing step, each detected beat has been marked as either good (high signal quality) or abnormal (low signal quality). If fewer than 80% of the

detected ABP beats are marked as high signal quality, the ABP signal quality for the 17 s segment is judged to be poor and the ECG alarm is accepted as true. If the signal quality for the segment is high, the logic employed to assess the validity of the alarm depends on the alarm type. Figure A-1 illustrates the algorithm architecture where the ABP signal quality is sufficiently high. The heart rate parameters found to be optimal by Aboukhalil *et al.* are summarized in Table A.3.

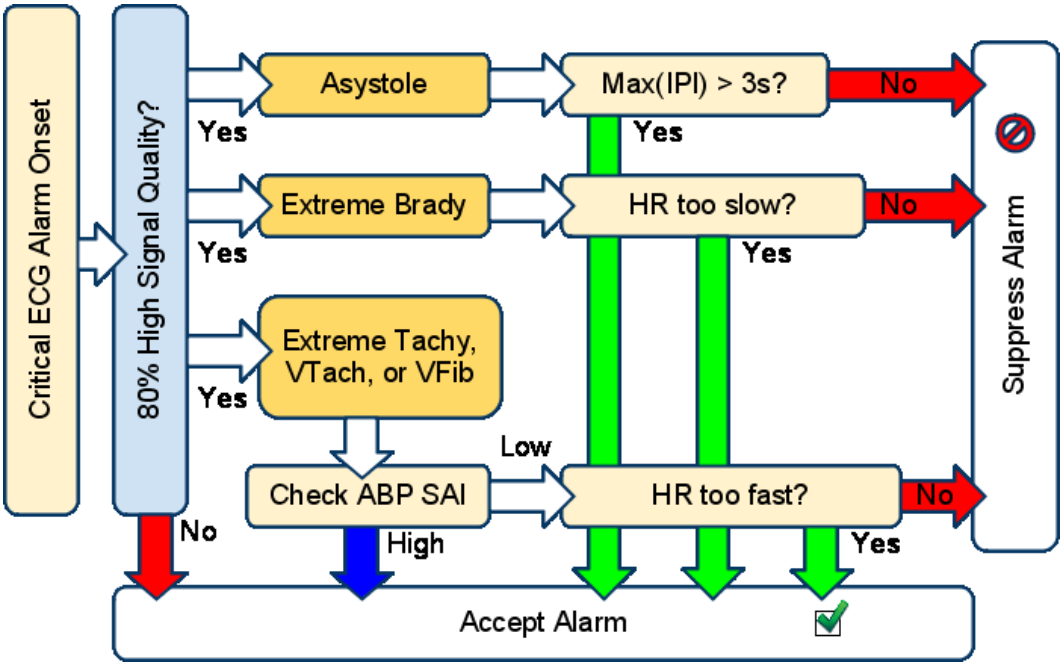

Figure A-1: False ECG Alarm Suppression Using the ABP Waveform. If at least 80% of the beats detected in a 17-second window are of high signal quality, logic is used to determine if the alarm should be accepted or suppressed. "IPI" stands for inter-pulse interval. "SAI" stands for signal abnormality index. Figure adapted from [1].

A.1.1 Asystole Processing

From the detected beat onsets, the largest beat-to-beat interval (for the case where the asystole resolves itself within the window) and the interval between the last detected pulse and the end of the window (for the case where asystole lasted beyond the analysis period) are calculated. If either of these intervals exceeds $T_A = 3$ s, the absence of beats is noted and the asystole alarm is accepted; otherwise it is suppressed.

A.1.2 Extreme Bradycardia Processing

Bradycardia alarms in the ECG waveforms are marked relative to a heart rate threshold set on the monitor. The $N_B = 3$ longest pulse-to-pulse intervals are calculated. If the mean heart rate calculated from these beats is within $E_B = 7$ beats per minute of the monitor's heart rate, then the bradycardia alarm is accepted; otherwise it is suppressed.

A.1.3 Extreme Tachycardia Processing

Tachycardia alarms in the ECG waveforms are marked relative to a heart rate threshold set on the monitor. The $N_T = 1$ shortest pulse-to-pulse interval is used to calculate the heart rate. If the heart rate estimate is less than $E_T = 20$ beats per minute over the threshold set on the monitor, and there are fewer than $M_T = 5$ abnormal beats lasting less than $T_T = 4$ s (indicating no period of abnormal beat morphology), then the tachycardia alarm is suppressed.

A.1.4 Ventricular Tachycardia Processing

A ventricular tachycardia alarm is accepted if the total duration of abnormal detected beats is more than $T_{VT} = 2$ s (indicating abnormal beat morphology) and the heart rate calculated from the $N_{VT} = 1$ shortest pulse-to-pulse interval exceeds $R_{VT} = 80$ beats per minute. Otherwise, the alarm is suppressed.

A.1.5 Ventricular Fibrillation Processing

Ventricular fibrillation alarms are suppressed if the total duration of abnormal detected beats is less than $T_{VF} = 2.5$ s (indicating no period of abnormal beat morphology) and the heart rate calculated from the $N_{VF} = 1$ shortest pulse-to-pulse interval is less than $R_{VF} = 150$ beats per minute. Otherwise, the alarm is accepted.

Table A.1: Performance of ABP-based false alarm suppression algorithm reported by Aboukhalil *et al.* The training set contained 267 alarms, and the test set contained 180 alarms. "FA" signifies false alarm. "TA" signifies true alarm. "FA Rate Before" and "FA Rate After" refer to the false alarm rate before and after the suppression algorithm was used, respectively. "-" indicates a value which was not reported.

Alarm Type	Data Set	TA Suppression	FA Suppression	FA Rate Before	FA Rate After
Asystole	Training	0%	92.5%	-	-
	Testing	0%	95.0%	-	-
	Combined	**0%**	**93.5%**	**90.7%**	**5.5%**
Ext. Brad.	Training	0%	79.7%	-	-
	Testing	0%	83.6%	-	-
	Combined	**0%**	**81.0%**	**29.3%**	**5.5%**
Ext. Tach.	Training	0%	59.4%	-	-
	Testing	0%	70.1%	-	-
	Combined	**0%**	**63.7%**	**23.1%**	**8.4%**
Vent. Tach.	Training	14.5%	28.3%	-	-
	Testing	4.0%	38.7%	-	-
	Combined	**9.4%**	**33.0%**	**46.6%**	**30.8%**
Vent. Fib.	Training	0%	57.7%	-	-
	Testing	0%	58.9%	-	-
	Combined	**0%**	**58.2%**	**79.6%**	**33.1%**
All	Training	4.7%	57.0%	-	-
	Testing	1.4%	63.2%	-	-
	Combined	**2.4%**	**59.7%**	**42.7%**	**17.2%**

A.1.6 Performance on Unseen Data

The performance of the false ECG alarm suppression system described above, as reported by Aboukhalil *et al.*, is summarized in Table A.1. This ABP-based system was also applied to the data described in Sections 2.3.1 and 2.3.2. The performance of the algorithm on the new MIMIC II data is summarized in Table A.2.

The ABP-based algorithm performed similarly on new data from the MIMIC II database as reported in the study of Aboukhalil *et al.*. The false alarm rate after applying the original ABP framework was higher on our data set for asystole alarms, as fewer false alarms were suppressed in this category than reported in the Aboukhalil's study. The false alarm suppression rate was also lower for extreme tachycardia and ventricular tachycardia alarms in our data set, and true alarm suppression rates were

Table A.2: Performance of ABP-based false alarm suppression algorithm on new MIMIC II data (described in Sections 2.3.1 and 2.3.2). Note that ventricular fibrillation/tachycardia alarms are combined with and annotated as ventricular tachycardia alarms. "FA" signifies false alarm. "TA" signifies true alarm. "FA Rate Before" and "FA Rate After" refer to the false alarm rate before and after the suppression algorithm was used, respectively.

Alarm Type	Data Set	TA Suppression	FA Suppression	FA Rate Before	FA Rate After
Asystole	Training	0%	70.9%	91.0%	26.5%
	Testing	0%	53.3%	90.0%	42.0%
	Combined	**0%**	**62.7%**	**90.5%**	**33.8%**
Ext. Brad.	Training	0%	90.6%	35.0%	3.3%
	Testing	0%	50.0%	16.1%	8.0%
	Combined	**0%**	**81.7%**	**27.8%**	**5.1%**
Ext. Tach.	Training	1.0%	54.6%	2.6%	1.2%
	Testing	0%	15.0%	12.9%	11.0%
	Combined	**0.7%**	**29.0%**	**5.3%**	**3.8%**
Vent. Tach.	Training	5.0%	26.7%	40.4%	29.6%
	Testing	10.8%	35.8%	54.9%	35.2%
	Combined	**8.0%**	**31.9%**	**47.6%**	**32.4%**
All	Training	3.2%	48.1%	36.9%	19.2%
	Testing	6.6%	40.2%	52.0%	31.1%
	Combined	**4.5%**	**44.0%**	**43.5%**	**24.4%**

non-zero for both extreme tachycardia and ventricular tachycardia (which was not observed in Aboukhalil's study).

A.1.7 Limitations

The ABP-based false alarm suppression system described by Aboukhalil *et al.* [1] had the poorest false alarm suppression rate (31.9%) on ventricular tachycardia alarms. Alarms in this category were also the only true alarms suppressed in the original study. The authors attribute the true ventricular tachycardia alarm suppressions to the observation that at low heart rates during ventricular tachycardia, the ABP morphology looks quite normal. Since the algorithm accepts ventricular tachycardia alarms if the calculated heart rate is over $R_{VT} = 80$ beats per minute and the total duration of detected abnormal pulses is more than $T_{VT} = 2$ s (indicating abnormal beat morphology), true ECG ventricular tachycardia alarms are suppressed when the corresponding ABP beats have normal morphology.

On our data set, the ABP-based algorithm also suppressed true extreme tachycardia alarms. In the ABP segments surrounding the suppressed true alarms, the pulses exhibiting rapid instantaneous heart rate have low pulse pressure and are not detected by $wABP$. The heart rate estimated from the detected pulses is therefore less than $R_T = 80$ beats per minute. The last detected pulse preceding the low-amplitude section is typically marked as having a long duration, but is the only abnormal beat (therefore the number of abnormal beats is less than $M_T = 5$). The duration of this one abnormal beat is less than $T_T = 4$ s. Because all three of these conditions are met from a non-sustained period of extreme tachycardia, the true tachycardia alarms are suppressed. This could be avoided either by introducing a threshold on the duration of the longest inter-pulse interval, or by reducing the number of abnormal beats or total duration of abnormal beats to account for unsustained episodes of tachycardia.

A.2 Modifications Made for Benchmarking

We used the performance of this ABP-based algorithm as a benchmark for the performance of the PPG-based false alarm suppression algorithm developed in this thesis. In order to reduce true alarm suppression, a modification has been made to the ABP-based algorithm. For each the three alarms related to fast heart rates (extreme tachycardia and ventricular tachycardia, and ventricular fibrillation), a new condition has been introduced regarding the longest inter-pulse interval. If the longest inter-pulse interval exceeds $T_{NoPulse} = 1.8$ s then the waveform indicates a temporary loss of pulse due to low stroke volume, resulting in some number of missed beat detections. The resulting algorithm architecture is as follows. Extreme tachycardia alarms are suppressed if the longest inter-pulse interval is less than $T_{NoPulse}$, the heart rate calculated from the shortest inter-pulse interval is less than $E_T = 20$ beats per minute over the monitor's declared heart rate threshold, and fewer than $M_T = 5$ abnormal beats lasting fewer than $T_T = 4$ s are detected. Ventricular tachycardia alarms are accepted if either the longest inter-pulse interval is greater than $T_{NoPulse}$ or both the total duration of abnormal detected beats is more than $T_{VT} = 2$ s and the heart rate calculated from the shortest pulse-to-pulse interval exceeds $R_{VT} = 80$ beats per minute. Ventricular fibrillation alarms are suppressed if the longest inter-pulse interval is less than $T_{NoPulse}$, the total duration of abnormal detected beats is less than $T_{VF} = 2.5$ s, and the mean heart rate calculated from the $N_{VF} = 1$ shortest pulse-to-pulse interval is less than $R_{VF} = 150$ beats per minute. The windowing and thresholding parameters are summarized in Table A.3.

A.2.1 Performance on Unseen Data

This modified system was applied to the data described in Sections 2.3.1 and 2.3.2. The performance of this modified ABP-based algorithm is summarized in Table A.4.

Modifying the ABP-based alarm suppression framework to detect loss in pulse volume decreased the true alarm suppression rate for extreme tachycardia alarms in the training set from 1.0% to 0.2% but increased the true alarm suppression rate in

Table A.3: Windowing and thresholding parameters in merged ABP-based false alarm suppression algorithm. "PPI" signifies pulse-to-pulse interval. "N/A" signifies that the parameter is not applicable.

Parameter ⇒ Alarm Type ⇓	Max. PPI length (s)	HR error margin (bpm)	Intervals for HR calc.	Duration of bad beats (s)	Abnormal beats allowed	Max. HR (bpm)
Asystole	$T_A = 3$	N/A	N/A	N/A	N/A	N/A
Extreme Bradycardia	N/A	$E_B = 7$	$N_B = 3$	N/A	N/A	N/A
Extreme Tachycardia	$T_{NoPulse} = 1.8$	$E_T = 20$	$N_T = 1$	$T_T = 4$	$M_T = 5$	N/A
Ventricular Tachycardia	$T_{NoPulse} = 1.8$	N/A	$N_{VT} = 1$	$T_{VT} = 2$	N/A	$R_{VT} = 80$
Ventricular Fibrillation	$T_{NoPulse} = 1.8$	N/A	$N_{VF} = 1$	$T_{VF} = 2.5$	N/A	$R_{VF} = 150$

Table A.4: Performance of modified ABP-based false alarm suppression algorithm on new MIMIC II data (described in Sections 2.3.1 and 2.3.2). Note that ventricular fibrillation/tachycardia alarms are combined with and annotated as ventricular tachycardia alarms. "FA" signifies false alarm. "TA" signifies true alarm. "FA Rate Before" and "FA Rate After" refer to the false alarm rate before and after the modified suppression algorithm was used, respectively.

Alarm Type	Data Set	TA Suppression	FA Suppression	FA Rate Before	FA Rate After
Asystole	Training	0%	70.9%	91.0%	26.5%
	Testing	0%	53.3%	90.0%	42.0%
	Combined	**0%**	**62.7%**	**90.6%**	**33.8%**
Ext. Brad.	Training	0%	90.6%	35.0%	3.3%
	Testing	0%	50.0%	16.1%	8.0%
	Combined	**0%**	**81.7%**	**27.8%**	**5.1%**
Ext. Tach.	Training	0.2%	54.6%	2.6%	1.2%
	Testing	0%	15.0%	12.9%	11.0%
	Combined	**0.2%**	**29.0%**	**5.3%**	**3.8%**
Vent. Tach.	Training	5.8%	25.2%	40.4%	30.2%
	Testing	10.4%	35.8%	54.9%	35.2%
	Combined	**7.8%**	**31.3%**	**47.6%**	**32.7%**
All	Training	2.9%	47.3%	36.9%	19.5%
	Testing	6.3%	40.2%	52.0%	31.1%
	Combined	**4.2%**	**43.6%**	**43.5%**	**24.6%**

the ventricular tachycardia category from 5.0% to 5.8%. The false alarm suppression rate for ventricular tachycardia alarms in the training set decreased slightly from 26.7% to 25.2%.

THIS PAGE INTENTIONALLY LEFT BLANK

Bibliography

[1] A Aboukhalil, L Nielsen, M Saeed, R G Mark, and G D Clifford. Reducing false alarm rates for critical arrhythmias using the arterial blood pressure waveform. *Journal of Biomedical Informatics*, 41(3):442–451, 2008.

[2] M Chambrin. Review: Alarms in the intensive care unit: how can the number of false alarms be reduced? *Critical Care*, 5(4):184–188, May 2001.

[3] G D Clifford, A Aboukalil, J X Sun, W Zong, B A Janz, G B Moody, and R G Mark. Using the blood pressure waveform to reduce critical false ECG alarms. In *Computers in Cardiology*, volume 33, pages 829–832, 2006.

[4] F M Coetzee and Z Elghazzawi. Noise-resistant pulse oximetry using a synthetic reference signal. *IEEE Transactions on Biomedical Engineering*, 47(8):1018–1026, August 2000.

[5] M Drinnan, J Allen, and A Murray. Relation between heart rate and pulse transit time during paced respiration. *Physiological Measurement*, 22(3):425–432, 2001.

[6] R Flewelling. Noninvasive optical monitoring. In JD Bronzino, editor, *The Biomedical Engineering Handbook*, pages 1346–1352. CRC Press, 1995.

[7] P T Gibbs, L B Wood, and H H Assada. Active Motion Artifact Cancellation for Wearable Health Monitoring Sensors using MEMS Accelerometers. *SPIE Smart Structures and Materials*, 5765:811–819, May 2005.

[8] E Gil, V Monasterio, P Laguna, and J M Vergara. Pulse photopletismography amplitude decrease detector for sleep apnea evaluation in children. In *27th Annual International Conference of the IEEE Engineering in Medicine and Biology Society*, volume 3, pages 2743–2746, 2005.

[9] E Gil, J M Vergara, and P Laguna. Detection of decreases in the amplitude fluctuation of pulse photoplethysmography signal as indication of obstructive sleep apnea syndrome in children. *Biomedical Signal Processing and Control*, 3(3):267 – 277, February 2008.

[10] A L Goldberger, L A N Amaral, L Glass, J M Hausdorff, P Ch Ivanov, R G Mark, J E Mietus, G B Moody, C-K Peng, and H E Stanley. PhysioBank, PhysioToolkit, and PhysioNet: Components of a new research resource for complex physiologic

signals. *Circulation*, 101(23):e215–e220, 2000. Circulation Electronic Pages: http://circ.ahajournals.org/cgi/content/full/101/23/e215.

[11] J Greenberg, J Fisher, W Wells, and G D Clifford. HST.582J / 6.555J / 16.456J Biomedical Signal and Image Processing. (Massachusetts Institute of Technology: MIT OpenCouseWare), http://ocw.mit.edu (Accessed July 2009). License: Creative Commons BY-NC-SA, Spring 2007.

[12] M J Hayes and P R Smith. Quantitative evaluation of photoplethysmographic artefact reduction for pulse oximetry. In *EUROPTO Conference on Medical Sensors and Fiber Optic Sensors IV*, volume 3570, pages 138–147, September 1998.

[13] B Hjorth. EEG analysis based on time domain properties. *Electroencephalography and Clinical Neurophysiology*, 29:306–310, 1970.

[14] B Hjorth. The physical significance of time domain descriptors in EEG analysis. *Electroencephalography and Clinical Neurophysiology*, 34:321–325, 1970.

[15] Q Li, R G Mark, and G D Clifford. Robust heart rate estimation from multiple asynchronous noisy sources using signal quality indices and a kalman filter. *Institute of Physics Physiological Measuremet*, 29:15–32, 2008.

[16] Q Li, R G Mark, and G D Clifford. Artificial arterial blood pressure artifact models and an evaluation of a robust blood pressure and heart rate estimator. *BioMedical Engineering OnLine*, 8(1):13, 2009.

[17] S P Linder, S M Wendelken, E Wei, and S P McGrath. Using the morphology of photoplethysmogram peaks to detect changes in posture. *Journal of Clinical Monitoring and Computing*, 20(3):151–158, June 2006.

[18] R G Mark. HST.542J / 2.792J / 20.371J / 6.022J Quantitative Physiology: Organ Transport Systems. (Massachusetts Institute of Technology: MIT OpenCouseWare), http://ocw.mit.edu (Accessed July 2009). License: Creative Commons BY-NC-SA, Spring 2004.

[19] G B Moody. *WAVE* user's guide. Available online at http://www.physionet.org/physiotools/wug/ (Accessed June 2009).

[20] G B Moody and R G Mark. A database to support development and evaluation of intelligent intensive care monitoring. *Computers in Cardiology*, 23:657–660, 1996.

[21] S. Nemati and Cifford G. D. Data fusion for improved respiration rate estimation. Technical report, Massachusetts Institute of Technology, January 2009.

[22] C F Poets and V A Stebbens. Detection of movement artifact in recorded pulse oximeter saturation. *European Journal of Pediatrics*, 156(10):808–811, 1997.

[23] M Saeed, C Lieu, G Raber, and R G Mark. MIMIC II: a massive temporal ICU patient database to support research in intelligent patient monitoring. *Computers in Cardiology*, 29:641–644, 2002.

[24] J W Severinghaus and J F Kelleher. Recent developments in pulse oximetry. *Anesthesiology*, 76(6):1018–1038, 1992.

[25] R Sokwoo, B H Yang, and H H Asada. Artifact-resistant power-efficient design of finger-ring plethysmographic sensors. *IEEE Trans Biomed Eng*, 48(7):795–805, 2001.

[26] J X Sun, A T Reisner, and R G Mark. A signal abnormality index for arterial blood pressure waveforms. *Computers in Cardiology*, 33:13–16, 2006.

[27] K K Tremper and S J Barker. Pulse oximetry. *Anesthesiology*, 70(1):98–108, 1989.

[28] L B Wood and H H Asada. Active motion artifact reduction for wearable sensors using Laguerre expansion and signal separation. In *27th Annual International Conference of the IEEE Engineering in Medicine and Biology Society*, pages 3571–3574, January 2005.

[29] L B Wood and H H Asada. Low variance adaptive filter for cancelling motion artifact in wearable photoplethysmogram sensor signals. In *29th Annual International Conference of the IEEE Engineering in Medicine and Biology Society*, pages 652–655, August 2007.

[30] M Yarita, N Kobayashi, S Takeda, and T Tamura. Compensation for two specific types of artifact in pulse wave using a Kalman filter. *Information Technology Applications in Biomedicine, 2007. ITAB 2007. 6th International Special Topic Conference on*, pages 269–272, 8-11 Nov. 2007.

[31] C Yu, Z Liu, T McKenna, A T Reisner, and J Reifman. A method for automatic identification of reliable heart rates calculated from ECG and PPG waveforms. *Journal of the American Medical Informatics Association*, 13(3):309–320, Jun 2006.

[32] W Zong, T Heldt, G B Moody, and R G Mark. An open-source algorithm to detect onset of arterial blood pressure pulses. *Computers in Cardiology*, pages 259–262, September 2003.

[33] W Zong, G B Moody, and R G Mark. Reduction of false arterial blood pressure alarms using signal quality assessment and electrocardiogram-arterial blood pressure relationships. *Medical and Biological Engineering and Computing*, 42, 2004.